Birzeit University

Faculty of Engineering and Technology

Joint Master Program in Electrical Engineering (JMEE)

Multi-Function Current Control Strategy for a Virtual Synchronous Generator

Prepared by:
Bahaa Abojams

1155461

Supervised by:

Dr. Muhammad Abu-Khaizaran and Dr. Mahran Quraan

This Master Thesis is submitted in partial fulfillment of the requirements for the Master Degree in Electrical Engineering

BIRZEIT
August 2020

Abstract

Recent trend of research is oriented toward different method of emulating the inertia of the synchronous generator to increase the reliability and stability of the power system in a micro grid. In the case of dynamic performance of power systems, especially in frequency control of interconnected systems, there are concerns considering the matter of virtual inertia. This thesis proposes a control technique for the virtual synchronous generator in a micro grid. Multipurpose control algorithm for integration of the distributed generator based on a conventional two level inverter is analyzed. The proposed control algorithm makes the system more stable and able to improve the power quality of the grid under real network challenges. The Distribution Generator (DG) will emulate the behavior of a synchronous generator, and replicate the stability and reliability introduced by the synchronous generator in the micro grid. The thesis presents an analytical study of the virtual synchronous machine employed as a distributed generation in a micro grid by modelling, control system, simulation results and discussion.

.

المستخلص

اتجهت الأبحاث في الآونة الأخيرة نحو عمل أنظمة لمحاكات عزم القصور الذاتي في المولدات التزامنية، بهدف زيادة استقرار وموثوقية نظام القدرة الكهربائية في الشبكات الصغيرة، في حالة الأداء الديناميكي لنظام القدرة الكهربائية خاصة في التحكم بالتردد للنظام الموصول، مع الاخذ بعين الاعتبار مسالة عزم القصور الذاتي. ان هذه الاطروحة تقدم تحليلا رياضيا ونظام تحكم لمولد تزامني افتراضي، يتعلق بعمل نظام تحكم متعدد الأهداف لربط مولدات التوزيع في الشبكات الصغيرة، نظام التحكم المقترح يزيد من كفاءة وموثوقية نظام القدرة الكهربائية، ويعمل على تنقية وتحسين التيار المسحوب من الشبكة الكهربائية. ان نظام المحاكاة في هذه الاطروحة يطبق على مولد احادي موصول على الشبكة، لتحقيق واثبات استقرار النظام وقدرته على مشاركة الاحمال الكهربائية.

Table of Contents

Acronyms and Abbreviations

APF	Active Power Filter
AVR	Automatic Voltage Regulator
DSTATCOM	Distribution Static Compensator
DPF	Displacement Power Factor
DG	Distribution Generator
PCC	Point of Common Coupling
PI	Proportional-Integral
PLL	Phase Locked Loop
PR	Proportional-Resonant
PF	Power Factor
VSI	Voltage Source Inverter
VSG	Virtual Synchronous Generator
SG	Synchronous Generator
THD	Total Harmonic Distortion

List of Figures

Chapter 1

Introduction

1.1 Overview

The expression of the Distribution Generator (DG) deals with any electrical power generation technology located beside the load centre and integrated to the electrical power network. It is cheap, efficient, reliable, and able to locate the electrical energy approximately next to the load center [1]. Therefore, the industrial consumer can gain various options in larger range of low cost and high reliability by using the DG technology.

Reactive power is an important component of the power flow in the power system. Reactive power is essential for operation of the large number of load either static or rotation load like induction motor. Therefore, in the transmission and distribution system of the electrical network the reactive power is an important component for a proper operation of the power system. The value and direction of the reactive power flow in the network vary according to the inductive load [2].

Reactive power flow has a number of undesirable consequences; it increases the current draw from the main source at the same load level, which increases the losses, maintenance and the cost of the power system operation. Therefore it mitigates the power quality of the system, and a heavy reactive power consumption causes instability of the voltage in the distribution system [3].

Due to increase of using the power electronic converters and other non-linear loads in industry, it is observed that the waveform of the current and voltage of the power system are

distorted. Static power electronic converters, such as single phase and three phase rectifiers, AC to AC converters and huge number of power electronics devices, are nonlinear loads, which generate significant disturbances in the main AC source. Therefore the power distribution problem increases due to the harmonics content generated by the nonlinear loads [4].

The percentage of distribution generator (DG) connected to the grid via inverters is growing rapidly in the worldwide. For example, 14.3 GW photovoltaic is planned to connected to the power grid in Japan by 2020, and 53 GW photovoltaic will be connected to the grid by 2030 [5]. The inverter used in the DG unit is controlled by a phase locked loop (PLL) in order to synchronize the DG unit with the grid frequency and phase angle. A power system become unstable when the percentage of the inverter based DG system becomes larger and larger, because the phase locked loop makes the inverter frequency determined by other synchronous generator. If the PLL loses the synchronism situation by the power system disturbances, the inverter probably loses the operation due to overvoltage on the DC side or overcurrent of AC side. So the inverter can operate as a synchronous machine using the concept of "Virtual Synchronous Generator" (VSG) by adding an algorithm to emulate the inertia in the control system of inverter.

Fig.1.1 shows a block diagram of the proposed system, which consists of Distributed energy source, a storage system, inverter, control system (Active Power Filter, D-STATCOM, VSG, and PLL), nonlinear load and grid. The conversion system is a simple DC/AC converter (inverter) that interfaces the DG with the grid. It converts DC power into a three-phase AC (or the other way round) using Pulse Width Modulation (PWM). Filters are added to reduce the voltage ripple (and hence, the current ripple) caused by switching.

The VSG control system has two main loops; the active power loop and reactive power loop. The active power loop emulates the machine's inertia, damping factor and frequency control of synchronous machine to generate the reference frequency and phase angle of modulating waves, while the reactive power loop emulates the voltage regulation to generate the magnitude of modulating waves.

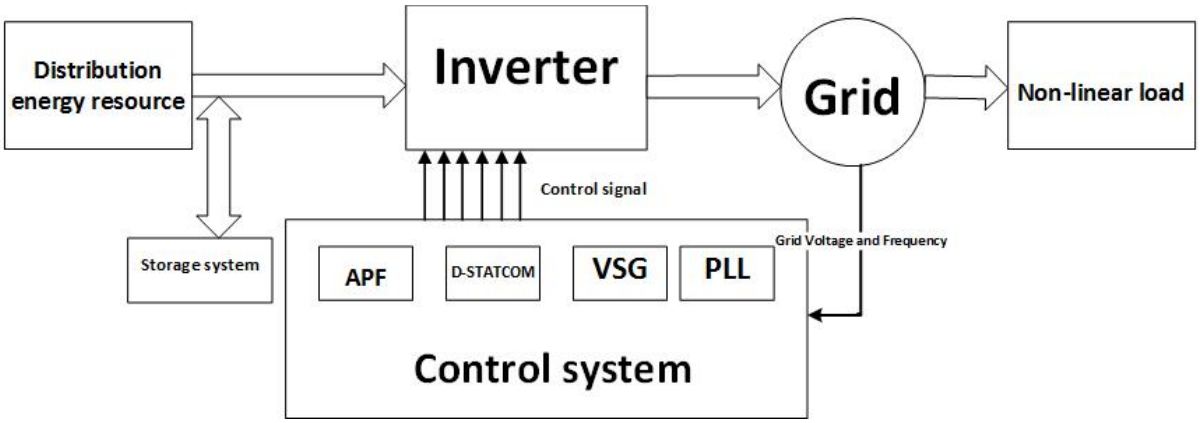

Fig. 1.1: The block diagram of the proposed system

The inverter is controlled to behave like a synchronous generator by the VSG control system to produce the speed-droop characteristics of the synchronous generator for load sharing. The output power of a VSG unit can be simply described using the swing equation as follows:

$$P_{VSG} = P_0 + K_i \frac{d\Delta\omega}{dt} + K_P \Delta\omega, \qquad \Delta\omega = \omega - \omega_0 \tag{1.1}$$

where ω_0 is the nominal frequency of the grid, P_0 denotes the primary power that should be transferred by the inverter. The second term indicates the amount of power that will be generated or absorbed by the VSG according to the positive or the negative initial rate of frequency change, K_i is the inertia emulating characteristic, and K_P is the droop coefficient and defines the power that needs to be absorbed or injected into the system due to the deviation of frequency from the reference value.

The control system of VSG can improve the grid stability c, because the VSG can provide a virtual inertia, which is similar to the actual rotor inertia in a real synchronous machine, by using a control algorithm and a storage system, and the continuous inverter operation on synchronized with other generator in the power system.

The VSG unit has the following functions:

- Measures the grid *abc*-phase voltages and currents
- Estimates the phase angle of the grid voltages and currents using a Phase Locked Loop (PLL)
- Performs the transformation of the *abc*-phase voltages to the synchronous reference in *dq*-domain
- Calculates the reference active and reactive power that should be produced by the VSG, considering the swing equation
- Determines the reference direct and quadrature currents
- Compares the reference direct and quadrature currents with the measured quantities to produce the reference direct and quadrature phase voltages
- Converts the reference direct and quadrature phase voltages to the *abc*-stationary reference frame
- Uses the reference modulated waves with an appropriate modulation scheme to run the inverter

Finally, the overall proposed system will be analytically modelled and then tested using Matlab/Simulink to demonstrate its main features.

1.2 Problem Statements

The presence of the harmonics in the power system causes high losses in distribution system, interference problems with the communication system, and causes improper operation of electronic equipment, which is very sensitive, because it contains micro controller system. Non-sinusoidal currents cause many problems in the main power and distribution system, such as low power factor, reduce the efficiency of energy, distorts of the voltage waveform etc. [4].

Most of the load in the electrical network are consuming reactive power due to presence of reactance. Heavy consumption of reactive power by the load causes poor quality of the voltage and decreases the power factor in the distribution system, which increases the maintenance and the operation cost of the power system. Today this problem has high impact on the reliability and security of the power system in the world and energy savers.

The presence of Synchronous Generator (SG) in a micro grid gives many of advantages in the field of stability and reliability in the power system. That is due to the inertia, load sharing and damping properties of the SG. When non-synchronous generator units replace a significant part of the synchronous generation capacity, the total inertia of the network is decreased significantly. This causes a large frequency variation in the power system with any change in the load, which produces unstable grid and frequency blackouts [6].

The solution of this problem to make the system more stable with the increase of penetration of the DG and Renewable Energy Sources (RESs) is to provide additional inertia virtually to emulate the behaviour of the synchronous generator. The virtual inertia can be added to the DGs/RES's by using a short-term storage system with the power electronics inverter and proper control system algorithm. This concept is known as Virtual Synchronous Generator (VSG) or Virtual Synchronous Machin (VSM) [7].

1.3 Publications

B. Abojams, M. Quraan, M. Abu-khaizaram," A Multi-Function Current Controller for a Virtual Synchronous Generator", 2020 International Symposium on Power Electronics , Electrical Drives and Motion, SPEEDAM 2020, Napoli ,Italy, pp. 654-658.

1.4 Research Goals

The objectives of this thesis are as follows:

- Demonstrate the structure and operating principle of the Virtual Synchronous Generator.
- Demonstrate the control algorithm of the active power filter.
- Demonstrate the control algorithm of the distribution STATCOM.
- To examine the proposed system using Matlab/ simulink and analyse the results.

1.5 Organization of The Thesis

This thesis is organised in six chapters and the rest of this thesis is organised as follows:

- Chapter 2 provides a review of main types of DGs system working as active power system and reactive power converter and supplying the real power to the load. The chapter also reviews the standard two-level inverter, which is commonly used as an interface system between the renewable energy resource and the grid.
- Chapter 3 introduces the operating principle of the DG with its mathematical model, and describes the mechanical part of the synchronous generator.
- Chapter 4 describes the control system of the conversion system including, the mechanical part of the synchronous generator.

- Chapter 5 presents simulation results considering the system without the converter, after the connection of the inverter to the system, and with increasing the nonlinear load.
- The last chapter concludes the work presented in this thesis and draws up some possible future works.

Chapter 2

Literature Review

This chapter reviews the main types of DGs system working as active power system and reactive power converter and supplying the real power to the load. The chapter also reviews the standard two-level inverter, which is commonly used as an interface system between the renewable energy resource and the grid.

The electric power system may experience sustained low frequency oscillations in the transmission line currents and voltages due to the lack of damping. Low frequency oscillation may cause the overcurrent of transmission line and mal-operation of the protection system [8], which affects reliability, dependability and stability of the electric power system operation. Nowadays, with the development of RESs, such as photovoltaic and wind power, many synchronous generators have been replaced by power electronic converters to generate a voltage level suitable for the grid connection. Due to the difference in grid-connected characteristics between power converters and synchronous machines, the RESs reduce the equivalent inertia and damping of the power system, and have negative effects on the power system stability [8] , [9].

2.1 Distribution Generator System

Distribution Generator (DG), with the inverter interface to the power system, is found in many green power applications. Most of RESs are interfaced to the electrical grid or local load by using DC to AC Pulse Width Modulation (PWM) current controlled Voltage Source Inverter

(VSI), because it's easy to implement and it contains a closed loop control for the current to reach the required operations [10].

Bapaiah [11], presents a discussion about the complete background of the device and power electronics application in the compensation equipment and also the modelling of the compensation using STATCOM is discussed. Wallace [12], presents an analysis of the performance and dynamic characteristic of a three phase active power filter operating with fixed switching frequency using a Pulse Width Modulation inverter .

Pouresmail [13], addresses a multi-objective control technique for integration of DGs to the electrical grid, the proposed strategy provides a compensation for active, reactive, and harmonic load currents components during connection of DG link to the grid. Naderi [14], presents a frequency-independent control method suitable for DGs using *abc*/*αβ and αβ/dq* transformations. Due the sensitivity of the PLL to noise and distortion, the elimination of PLL function can bring benefit for robust control against distortion in DG application.

2.2 Virtual Synchronous Generator

The concept of virtual synchronous generator describes a new type of grid feeding inverter, which operates with a storage system entirely as an electromechanical synchronous machine. The basic idea of the VSG is to reproduce the static and dynamic properties of a real synchronous machine on a power electronic interface between a distributed generator (DG) unit and the grid, in order to inherit the advantages of a synchronous machine in consideration of power system stability such as adjustable active and reactive power, dependence of the grid frequency on the rotor speed and the effect of the rotating mass and damper windings as well as stable operation with a high parallelism level.

In [15], a new approach for implementing the virtual inertia in a two area AC/DC interconnected system is proposed. Derivative control technique is used to control the stored energy of converter devices in AC/DC interconnected Automatic Generation Control (AGC) to the power system. Reference [16], proved that the VSG has a better frequency stability because it possess inertia larger than the droop control, and the amount of inertia depends on virtual moment of inertia (J), whereas the damping ratio depends on damping factor (D) and the output of reactance. However, the active power of VSG is more oscillatory than the droop control[17]. This problem can be resolved by tuning the damping factor and/or the output reactance. In [18], the alternating inertia structure was elaborated, the alternating inertia scheme adopted the suitable value of the moment of inertia of the VSG considering, its virtual angular velocity and acceleration/deceleration in each phase of oscillation is considered. In [19], the synchronous generator emulation control strategy is proposed for the VSG station, the control scheme is divided into two separated loops: an inner control loop and an outer control loop. The inner controller is a conventional vector controller developed for the fast current control and the point of common coupling (PCC) voltage regulator. In the outer controller, the conventional droop control is modified by introducing a first-order inertia element, the vector current controller included in the system is effective in preventing the VSC from over-current blocking during system disturbances as shown in Fig. 2.1.

In [5], the concept of controlling an inverter to behave like a synchronous generator is studied, a control system for VSG, which solves the output power oscillation, occurred due to the characteristic of the simulated synchronous generator, is proposed. In [17], the authors presented A review of the fundamental and main concept of VSGs and their role to support the

power grid control.

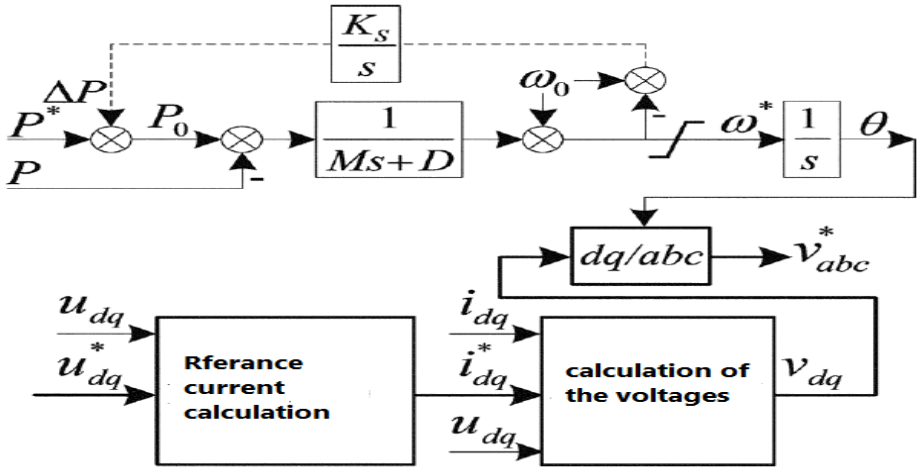

Fig. 2.1: A Synchronous Generator Control Strategy

In [20], a detailed modelling of a configuration of a grid-connected Voltage Source Inverter (VSI), controlled as Virtual Synchronous Machine (VSM), is presented. The VSM inertia emulation is based on the swing equation of a traditional synchronous machine, which provides a power balance, based synchronization of the converter control system with the grid. In [21], an active power controller, which enables a grid-connected converter to interact synchronously with the power system and at the same time controls the converter DC link voltage is presented. A power converter equipped with this controller can be identified as a conventional synchronous generator, which synchronizes itself with an existing power system or is able to form it's own grid. The synchronization does not need an additional PLL, since the phase angle of the currents produced by the converter determined by a power balance equation analogous to the swing equation of a synchronous generator. In [22], an adaptive structure for real time selection of a suitable value for the moment of inertia of a VSG considering its virtual angular velocity and acceleration/deceleration in each phase oscillation, is proposed. In [23], the island-mode of the VSM is investigated and validated by simulation and experiment results.

Two cases for island mode of the VSM are considered; one of them is that, the VSM works firstly parallel with the main grid and then the main grid is lost. Another case is that the VSM makes a stand-alone grid by itself without being connected to any other grid. In [24], the concept of controlling an inverter to behave like a synchronous generator is presented. The VSG enhances grid stability because VSG has a virtual inertia and the VSG control scheme to use the swing equation of a synchronous generator was presented where in article [25], the dynamic properties of VSM system pointed out the effect of virtual mass and damping is presented. Reference [26], introduces the VSM concept to upgrade grid-feeding inverter with synchronous machine behavior to improve the power quality and stability of the grid. In [27], the inertia emulation is achieved by a proper choice of control parameter of a PLL, and the rotor speed transient excursions can be significantly damped without extensive VSG power budget penalty. In [28], a Virtual Synchronous Machine (VSM) concept contains the virtual machine algorithm, to let any DC feeding generators, preferable wind, solar, fuel cell or Combined Heat and Power (CHP) system, appear and operate entirely as a synchronous machine connected to the grid.

This thesis will address modelling and test of the multi-function current control strategy using virtual synchronous generator-based grid-interface converters for renewable energy systems integration. The importance of this topic is reflected in recently published articles [6].

Chapter 3

Conversion System

This chapter introduces the construction and the basic principle of operation of the main part of the overall system including the grid, the inverter system, the filter, the nonlinear load and the conversion system between three phase system and dq0 and αβ systems. It also presents the dynamic model of some modulation strategies used for driving the inverter. Finally, it presents the model of the two level inverter and the electromechanical model of the synchronous generator.

3.1 Inverter Structure and Operating Principle

3.1.1 Three Phase Voltage Source Inverter Topology

The three phase inverter is a power electronic circuit that converts the DC voltage or current into three phase AC voltages or currents to supply a load that operates on AC voltages or currents. The output of the inverter consists of a fundamental component and harmonics [29]. The topology of three-phase voltage source inverter is shown in Fig. 3.1.

The switches in a VSI have ability to conduct current in both direction (upwards and downwards). Therefore, each switch has anti parallel diode either external fast recovery diode or a body diode of the MOSFET. Furthermore, a dead time (underlap period) between switches in the same leg must be considered, where both switches are off. This time must elapse before turning on the off-switch. The range of the dead time is typically from 1μs to 5μs, depending

on the switching speed of the switch, power level, and the circuit topology. The conventional numbering sequence of the switches represents the operation sequences of switches [30].

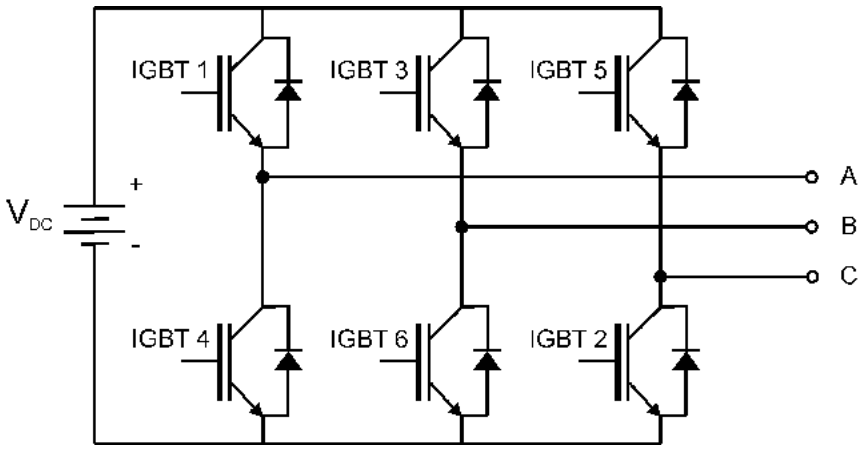

Fig. 3.1: Two level three Phase Inverter

3.1.2 Sinusoidal Pulse Width Modulation (SPWM) in a Three-Phase Voltage Source Inverter

One of the most popular modulation technique of inverter for harmonics reduction is Sinusoidal Pulse Width Modulation (SPWM). SPWM schemes relies on comparing a three sinusoidal control signals which are 120 degree out of phase from each other, with a common triangular voltage to produce the gate signals for switches (IGBT) in the respective leg [31]. SPWM can be generated either by microcontroller/ microprocessors or by using a chip like MA828. The switching waveforms are shown in Fig. 3.2.

SPWM technique contains of strain of constant amplitude pulses with different duty cycle for each switching period. The frequency of the sinusoidal control signal is chosen according to the output voltage frequency of inverter, and the frequency of the triangular wave represents the switching frequency of the semiconductor devices (IGBT's), which is usually high frequency (serval kHz., Moreover, the amplitude of the control signal is reflected on the amplitude of the output voltage.

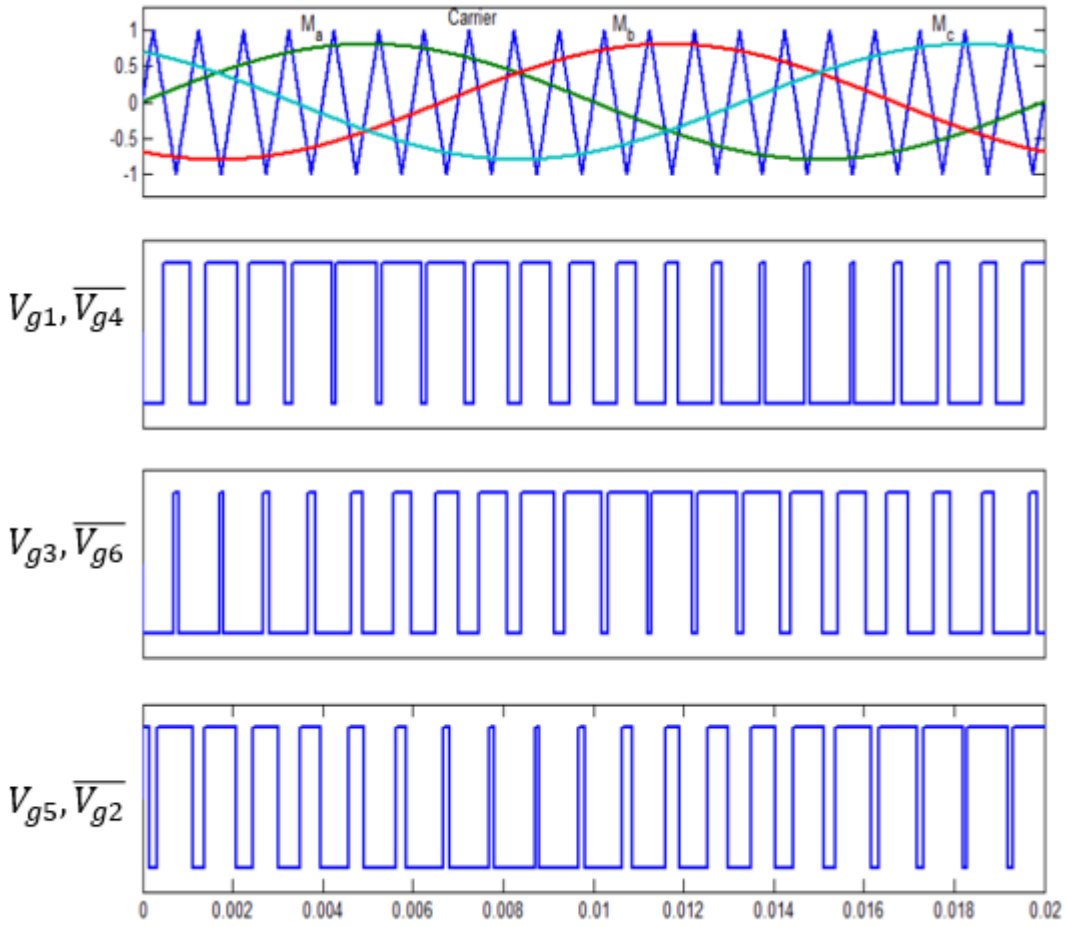

Fig. 3.2: Example of SPWM generation signal [32]

The resulting fundamental line-to-line voltage (V_{AB}) leads the phase to neutral voltage (V_{AN}) by 30 degree, which is consistent with three-phase concept, and the peak value of the fundamental component of phase voltage is given by :

$$\widehat{V_{AN}} = M\frac{V_{dc}}{2} \tag{3.1}$$

where M is the modulation index, and $V_{dc}$is the DC link voltage.

The amplitude modulation index or ratio (M) is defined as:

$$M = \frac{\widehat{V_c}}{\widehat{V_{tri}}} \tag{3.2}$$

where $\widehat{V_c}$is the amplitude of the sinusoidal control signal, and $\widehat{V_{tri}}$ is the maximum voltage level of the triangular voltage

Thus, the amplitude of the fundamental component of the line-to-line voltage is:

$$\widehat{V_{LL}} = \sqrt{3}M\frac{V_{dc}}{2} = 0.866MV_{DC} \quad (3.3)$$

Therefore, the output line-to line voltage between the phase A and B is:

$$V_{AB}(t) = 0.866MV_{DC}\sin\left(\omega_1 t + \frac{\pi}{6}\right) + Harmonics \quad (3.4)$$

3.1.3 Filter Design

The power quality of the grid connected inverter is dependent on the quality of injected currents. The quality of the current is regulated by the utility company; for example the total demand distortion (TDD) of the average injected current should not exceed 5% [32] .

$$TDD = \sqrt{\sum_{h=2}^{\infty} I^2(h)/I_{rated}} \quad (3.5)$$

The order of the harmonics depends on the switching frequency of the utility inverter, which comes from the condition between the grid voltages and PWM switching pattern. The current ripple caused by the switching frequency of the inverter can be attenuated by a passive filter. The current ripple can be evaluated by a ripple factor as defined in (3.6) [33]. A low pass filter is connected at the output of inverter. A simple L-type filter is shown in Fig. 3.3.

$$RF = \frac{\sum I(h)}{I_{rated}} * 100\% \quad (3.6)$$

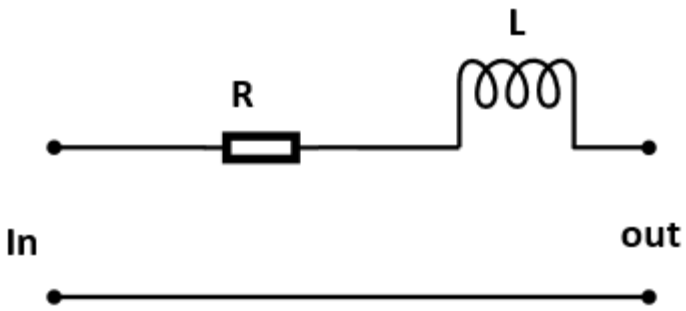

Fig. 3.3: L-type Filter circuit diagram

Filter Design Guideline for Full-Bridge Topology:

The fundamental component of the filter inductor current of the single phase full bridge grid connected inverter can be calculated by (3.7) [32].

$$I_1 = \frac{Mv_{dc}}{\sqrt{2}z_{base}} = \frac{M_a T v_{dc}}{2\sqrt{2}\pi L_b} \tag{3.7}$$

where T is the period of the injected current at fundamental frequency.

The switching ripple factor of the grid connected single phase full bridge inverter is calculated by (3.8) [32].

$$RF_{sw} = \frac{I_r}{I_1} = \sqrt{\frac{\pi}{3}\left\{\frac{\pi}{4}\left(1+\frac{3}{4}M^2\right)-\frac{4}{3}m\right\}}.\frac{T_s}{T}.\frac{L_b}{L} \tag{3.8}$$

where I_r is the rated current, T_s is the switching time and $L_b$is the boundary inductance.

Therefore, when RF_{sw} gives the ripple factor of the injection current, the filter inductor must be designed by eq.9 [32].

$$\frac{L}{L_b} \geq \frac{1}{RF_{sw}}\sqrt{\frac{\pi}{3}\left\{\frac{\pi}{4}\left(1+\frac{3}{4}M^2\right)-\frac{4}{3}M\right\}}.\frac{T_s}{T}\ [pu] \tag{3.9}$$

3.2 Phase Locked Loop

The Synchronous Reference Frame (SRF) Phase Locked Loop (PLL) is important and is a sensitive part for control and synchronizing the three-phase grid connected inverter to the power system. A typical digital system of the PLL is constructed from three components; phase detector (PD), loop filter (LF) and digital control oscillator. Generally, the main difference between the structure of various PLL is by the way of implementation of the PD [34].

The wildely used three-phase SRF PLL system is shown in Fig. 3.4; it is constructed from an abc/dq transformation block as PD, to convert the positive sequence of the voltage that is measured by eq.10 to the q-component. The positive sequence (PS) voltage can be found by different PS detectors, so that the zero and negative sequence of the grid voltage will not affect to the tracking of the phase [35].

$$\begin{bmatrix} V_{ga} \\ V_{gb} \\ V_{gc} \end{bmatrix} = \begin{bmatrix} V_g \cos(\theta_g) \\ V_g \cos\left(\theta_g - \frac{2}{3}\pi\right) \\ V_g \cos\left(\theta_g + \frac{2}{3}\pi\right) \end{bmatrix} \tag{3.10}$$

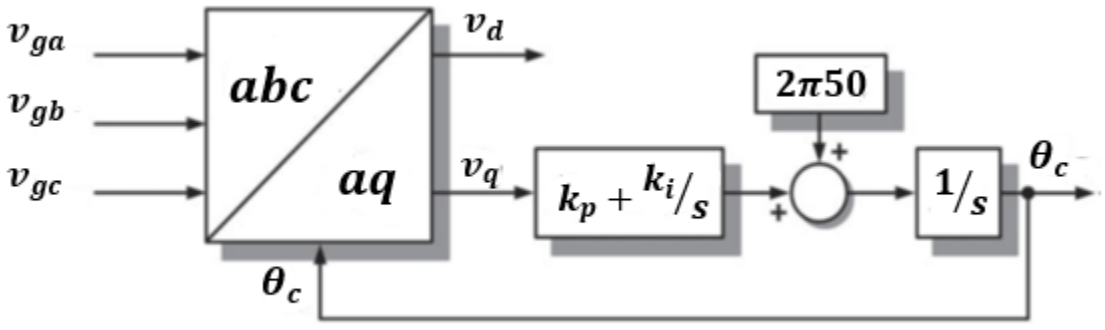

Fig. 3.4: The SRF. PLL

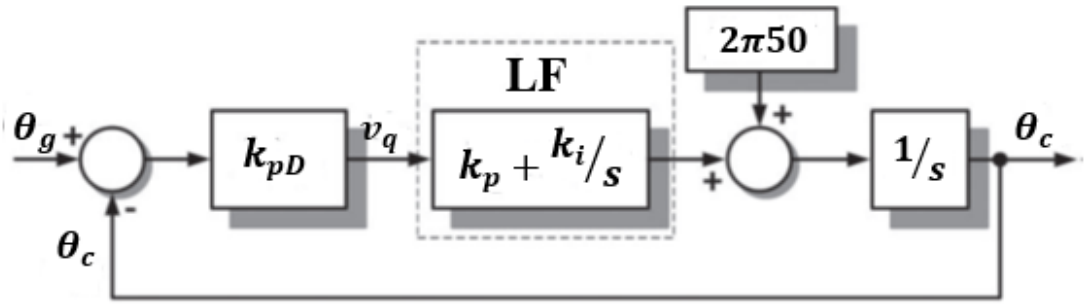

Fig. 3.5: The typical linearized PLL model

Fig. (3.5) represents a typical linearized PLL model [34]. The q-component of the voltage signal v_q, is the phase error signal. The PD gain K_{PD} that shown in (3.11), is equal to the amplitude of the input voltage. This model is very popular in the PLL design. However, it is unable to explain the nonlinear behaviors under the islanding and weak grid condition [34].

$$v_q = V_g \sin(\theta_g - \theta_c), \qquad K_{PD} = \frac{\widetilde{v_q}}{\tilde{\theta}} = V_q \tag{3.11}$$

3.3 Nonlinear Load and Harmonics in Power System

A nonlinear load in a power system is characterized by the introduction of a switching action and consequently current interruptions. This behavior provides current with different components that are multiples of the fundamental frequency of the system. These components are called harmonics. The amplitude and phase angle of a harmonic is dependent on the circuit and on the load it drives. For example, if the current draw from the source has a square wave shape, then the current may be synthesized from a fundamental component, and other high frequency components as illustrated in Fiq.3.6. For a fundamental power frequency of 50 Hz, the 3rd harmonic is 150 Hz, the 5th harmonic is 250 Hz, and so on. The harmonic currents flow toward the power source through the path of least impedance.

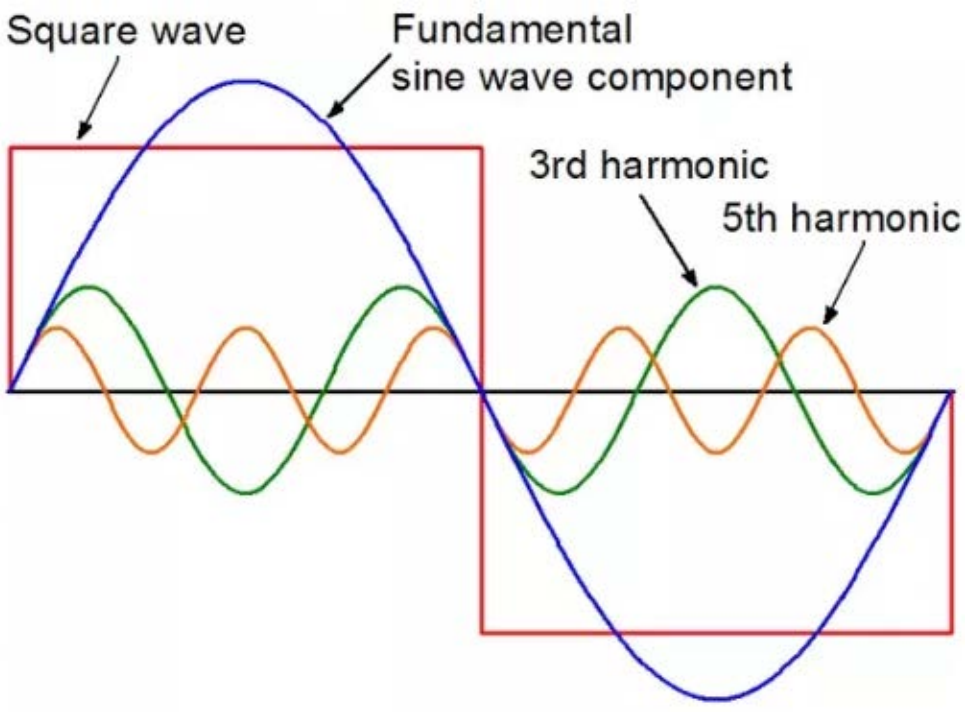

Fig. 3.6: Fundamental and harmonic components of the square wave signal

3.3.1 Power and Harmonics in The Power System

For a sinusoidal voltage, the current harmonics do not affect the average load power. However, the current harmonics increase the RMS current, and thus the power factor decreases. The average power is given in (3.12), and the RMS current, by considering the harmonics is given in the (3.13) [36].

$$P_{avg} = \frac{V_1 I_1}{2} \cos(\varphi_1 - \theta_1) \tag{3.12}$$

$$I_{RMS} = \sqrt{I_{avg} + \sum_{h=1}^{\infty} \frac{I_h^2}{2}} \tag{3.13}$$

where $V_1 and\ I_1$ are the peak value, $\varphi_1 and\ \theta_1$ are the phase angle of fundamental voltage and current respectively and I_h is a peak current at the harmonics number h. power factor of the system is given in the eq.14 [36].

$$Power\ Factor = \sqrt{\frac{I_1/\sqrt{2}}{I_{avg}^2+\sum_{h=1}^{\infty} I_h^2}}\cos(\varphi_1 - \theta_1) \tag{3.14}$$

= (Distortion Factor) (Displacement Power Factor)

where the distortion factor is defined as the ratio of fundamental RMS current to the total RMS current. The total harmonic distortion (THD) which is the harmonic index is defined in (3. 15) and the distortion factor in the term of THD is given in (3.16).

$$THD = \frac{\sqrt{\sum_{h=2}^{\infty} I_h^2}}{I_1} \tag{3.15}$$

$$Distortion\ Factor = \frac{1}{\sqrt{1+(THD)^2}} \tag{3.16}$$

The single-phase nonlinear load, as electronic ballast or a personal computer, generates odd harmonics (3rd, 5th, 7th, 9th, etc.). The triplen harmonics (3rd order and its odd multiples) make an overload to the neutral conductor in a 3-phase system, because they will add the harmonics in every phase rather than cancel on the neutral conductor. Furthermore, the triplen harmonics produce a circulating current in the delta winding of a delta-star transformer, that causes a heating of the transformer similar that produced by unbalance 3-phase system [36].

On the other hand, 3-phase nonlinear loads like 3-phase DC-drives, rectifier, Adjustable Speed Drives (ASD), etc. do not generate a triplen harmonics in the current, these type of loads generate primarily 5th, 7th current harmonics, and higher order based on the configuration of the converter [37].

3.3.2 Modelling of The Industrial Loads

The industrial nonlinear load produces a harmonic current flowing in the utility grid. This may cause a malfunction of the sensitive loads that are connected at the Point of Common Coupling (PCC). The most popular way to analyse the harmonics is the computer simulation by modelling the system components and studying it either through measurement or mathematically. In this way, the harmonic currents injected by an industrial at PCC can be estimated.

The Florescent lamp has a negative resistance dynamics behaviour. The electronic ballast contains a half bridge inverter and an LC filter used to acquire the nonlinear characteristic of the lamb [37].

The Adjustable Speed Drive (ASD) consists of a variable AC voltage converter driving an AC motor. The ASD consists of three main component; a 6 or 12 pulse rectifier, inverter stage that converts the DC voltage to a controllable frequency AC voltage to control the speed of the motor, and a DC link (shunt capacitor) that couples the two main stages and reduces the ripple of the DC voltage. Therefore, three-phase bridge converter with DC link circuit can model the ASD.

The most popular load in the modern life is the personal computer. It generates harmonic currents especially when used in large concentration in a distribution system. It utilizes the technology of the switch mode power electronics, which draws the nonlinear current that contains a large amount of third and higher order harmonic currents.

A typical PC load model consists of a full wave rectifier, DC storage capacitor ”c”, diode bridge resister and a series Radio Frequency Interference (RFI) chock, which is represented by

inductance L. Fig. 3.7 shows the current waveform and FTT analysis of the three phase full wave rectifier when modelled in the Matlab/Simulink program.

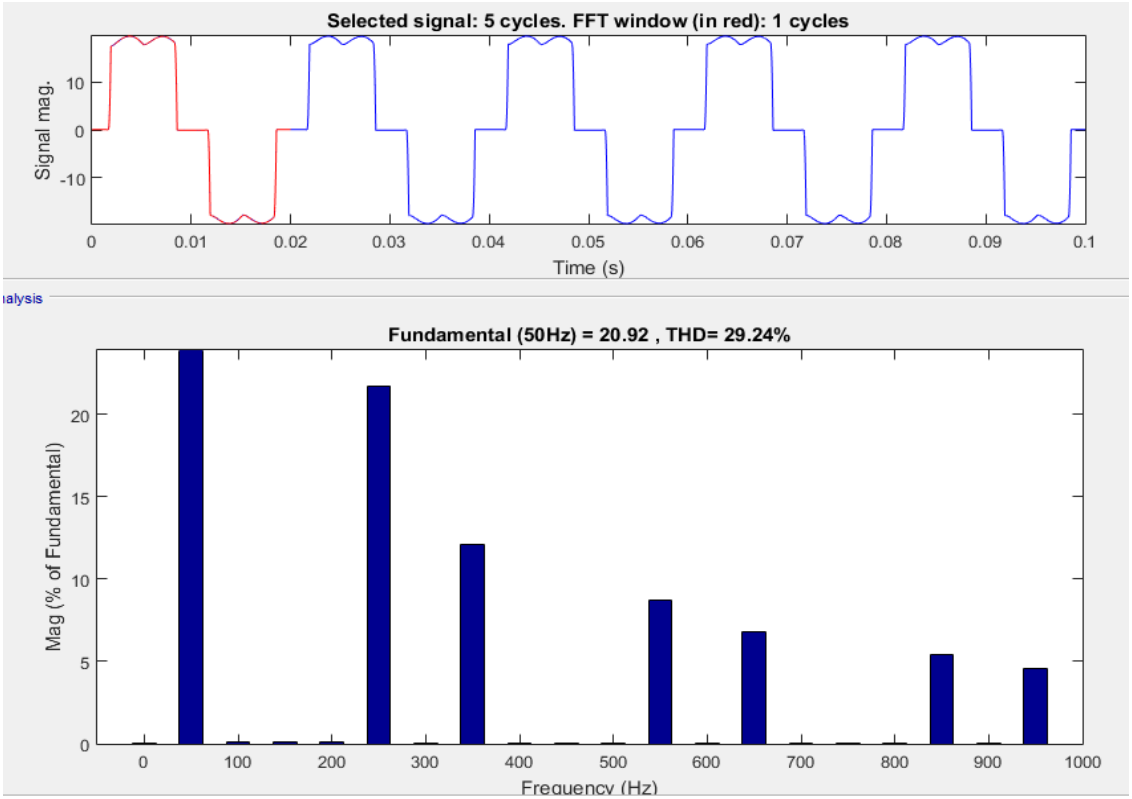

Fig. 3.7: Simulated current waveform and harmonics spectrum for a 3-phase full wave rectifier

3.4 Three Phase Representation

3.4.1 abc Sequence

The abc sequence is the usual method to express the three-phase voltage, current, and other parameters. The phase sequence is shown in Fig.3.8.

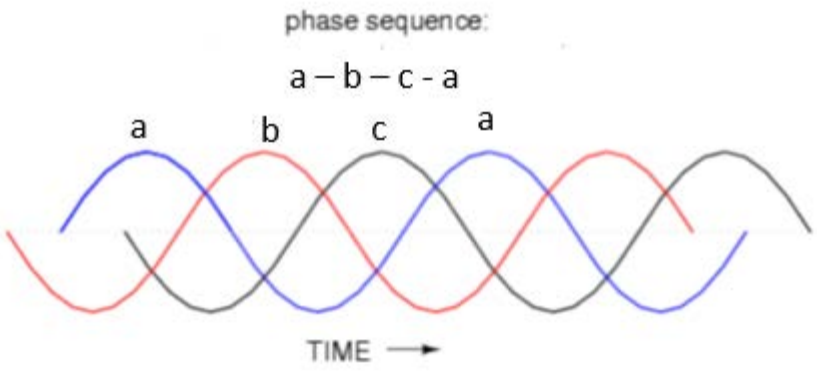

Fig. 3.8: abc sequence in time domain

The phasor diagram of the three-phase system expressed in abc sequence is shown in Fig. 3.9.

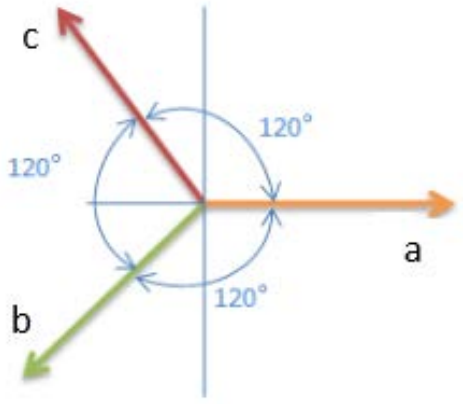

Fig. 3.9: The phasor diagram of abc sequence

3.4.2 Reference Frame Representation

The alpha-beta (α, β) transformation (Clark Transformation), is a mathematical transformation used to simplify the analysis of a three-phase system. The quadrature-direct-zero (dq0) transformation is a tensor that rotates the reference frame of the three element vector or 3*3 matrix in an effort to simplify the analysis. The dq0 component can be calculated by the product of Clark and Park transformation [38]. Fig 3.10 shows the three-reference frames of the three phase currents.

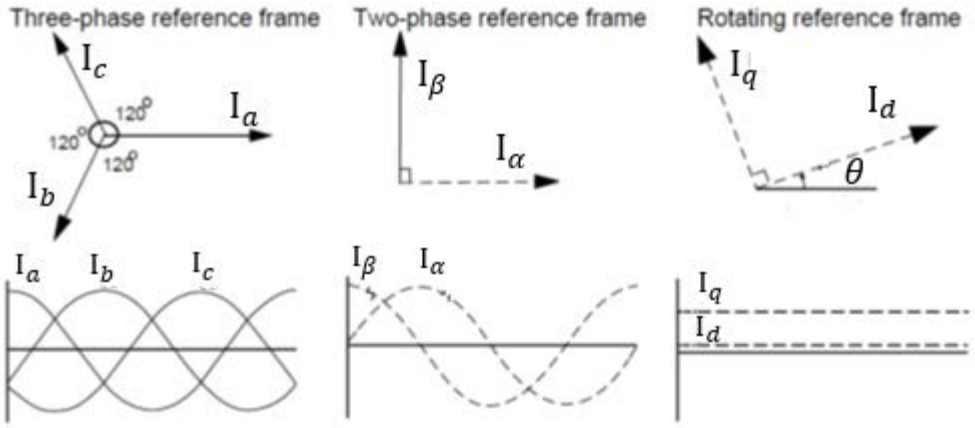

Fig. 3.10: Three phase current Reference Frame Representation.

The conversion of three-phase system from stationary to a synchronous frame, can be done using the following procedure [39] , [40]:

- Convert the three phase system into two axis (α and β) by applying the Clark transformation matrix in (3.17). In the other words, the three-phase system component are projected onto two orthogonal axis system (X_α, X_β) as shown in Fig. (3.11).

$$\begin{bmatrix} X_\alpha \\ X_\beta \end{bmatrix} = \begin{bmatrix} 1 & -1/2 & -1/2 \\ 0 & \sqrt{3}/2 & -\sqrt{3}/2 \end{bmatrix} \begin{bmatrix} a \\ b \\ c \end{bmatrix} \tag{3.17}$$

where a, b and c is the three phase stationary frame components, and X_α and X_β are the components projected onto the two stationary orthogonal axes.

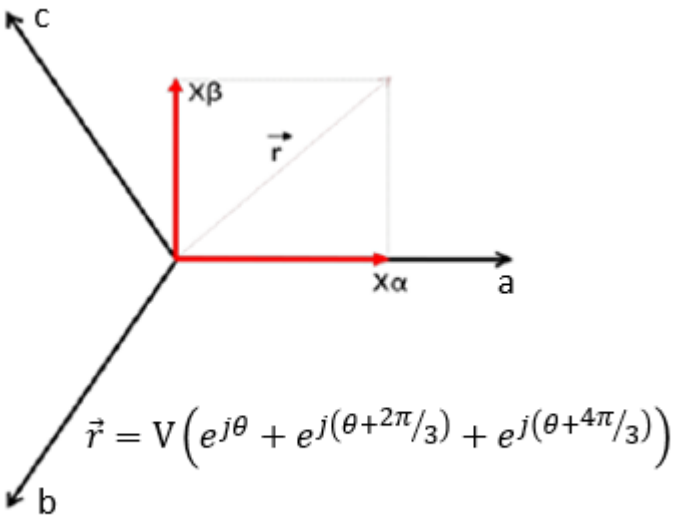

Fig. 3.11: Clark transformation vector [40]

- Transform the two-axis component (X_α, X_β) from stationary to synchronous rotating frame (d and q axis) that rotates at the angular velocity (ω). This make the synchronous rotating frame represent a stationary frame with relative to the angular velocity of the system. So that the AC variables (voltage and current) become time invariant at the fundamental frequency. The Park transformation matrix in (3.18) performs the transformation between the stationary and rotating reference axis (X_d and X_q), as shown in Fig. (3.12).

$$\begin{bmatrix} X_d \\ X_q \end{bmatrix} = \begin{bmatrix} \cos(\omega t) & \sin(\omega t) \\ -\sin(\omega t) & \cos(\omega t) \end{bmatrix} \begin{bmatrix} X_\alpha \\ X_\beta \end{bmatrix} \quad (3.18)$$

This transformation make a new frame components which are time invariant in the rotating reference frame, and rotating with angular velocity ω.

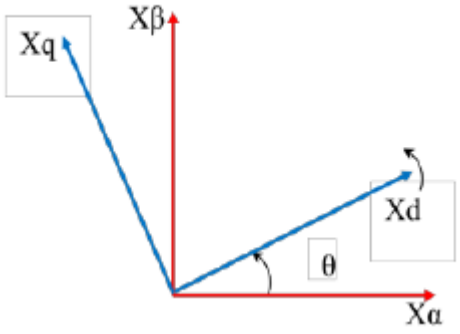

Fig. 3.12: Park transformation [40]

The transformation and reference frame theory is interesting in the control strategies of the voltage source inverter, because of the following points [13], [40], [41].

- This transformation makes the electrical quantity time invariant (at the fundamental frequency). So that, the feedback control can be demonstrate by using the PI controller in an efficient manner.
- The transformation enable the use of solid-state inverter for the grid connected inverter application, in which the transformation theory is already used for it control.
- The demonstration of the digital control becomes powerful, practical and the cost of implantation in this technique is dropped. They are also popular in industrial applications.
- Space Vector Modulation (SVM) is the most effective switching strategy of voltage source inverter when implementing this transformation [42],[43].

3.5 Modeling of The Inverter System

A schematic diagram of the proposed DG model is shown in Fig. 3.13. The system contains a utility grid (infinite bus system), a conventional Voltage Source Inverter (VSI) and a nonlinear load. The transmission line up to the point of common coupling is represented by a series inductance and resistance (R_S, L_S). The transformer and the filter of the VSI is represent by the coupling inductance and resistance (R_C, L_C). Sinusoidal Pules Width Modulation (SPWM) is used to generate the appropriate gate pulses to the IGBTs. The VSI in the model will be controlled in a manner emulating a Virtual Synchronous Generator (VSG).

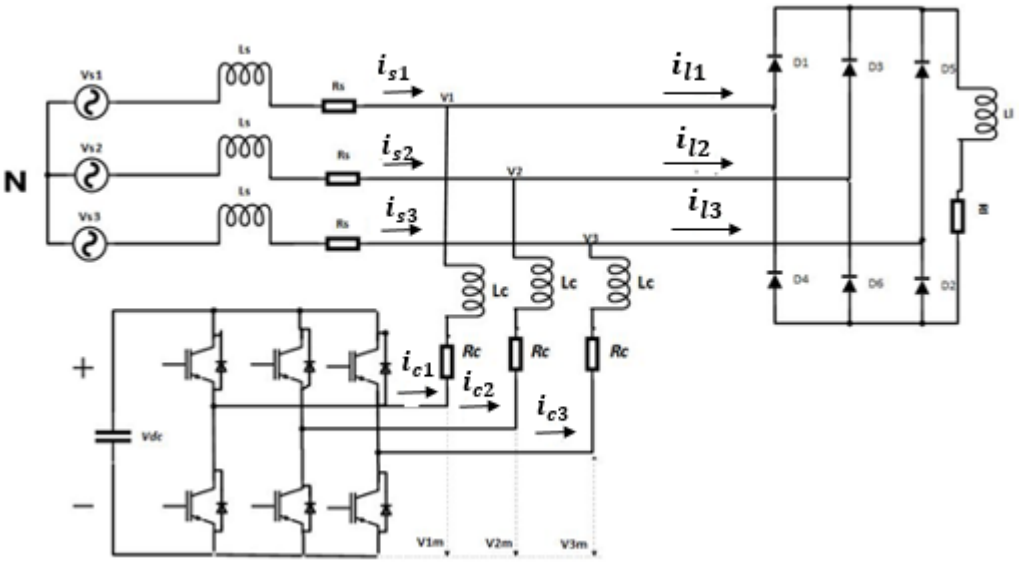

Fig. 3.13: Schematic diagram of the DG proposed model

3.5.1 Mathematical Modelling of The Propose DG System

According to Fig. 3.14, the electrical grid includes the generation system, the transmission line, distribution system, and the load. The DG unit is an additional component in the electrical network and is represented by a DC voltage source connected to the proposed converter.

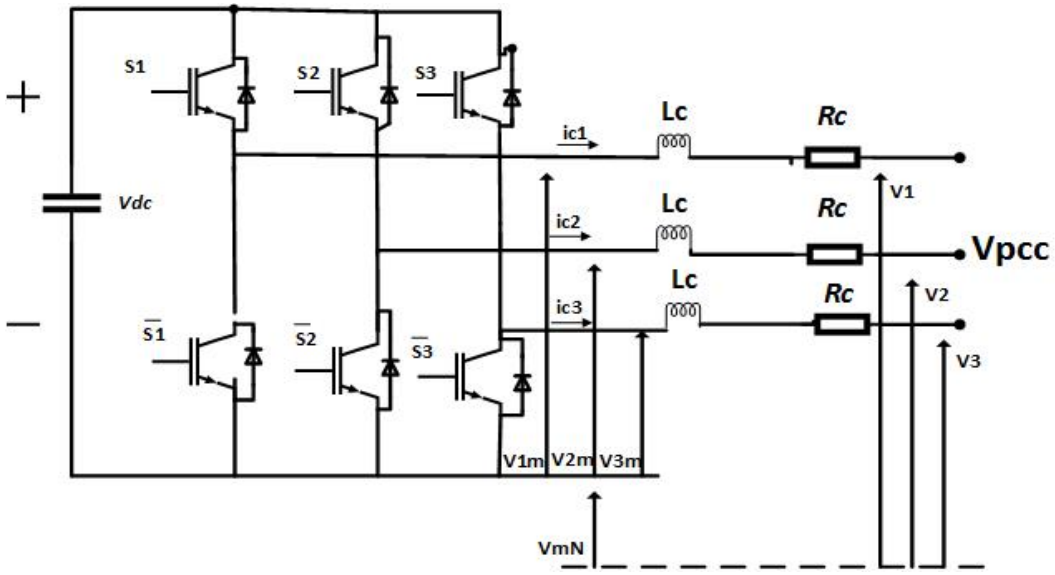

Fig. 3.14: : Equivalent circuit of the DG proposed system

To draw the appropriate plan to control the interface system of the VSI connected to the power plant, dynamic model analyses of the proposed system should be developed.

According to Fig. 3.14, and by applying the KVL for the load voltage at the Point of Common Coupling (PCC), which leads to:

$$\begin{aligned} -V1 - L_C\frac{di_{c1}}{dt} - R_c i_{c1} + V_{1m} - V_{Nm} = 0 \\ -V2 - L_C\frac{di_{c2}}{dt} - R_c i_{c2} + V_{2m} - V_{Nm} = 0 \\ -V3 - L_C\frac{di_{c3}}{dt} - R_c i_{c3} + V_{3m} - V_{Nm} = 0 \end{aligned} \quad (3.19)$$

Rearranging (3.19), yields:

$$\begin{aligned} V_{1m} = L_C\frac{di_{c1}}{dt} + R_c i_{c1} + V_1 + V_{Nm} \\ V_{2m} = L_C\frac{di_{c2}}{dt} + R_c i_{c2} + V_2 + V_{Nm} \\ V_{3m} = L_C\frac{di_{c3}}{dt} + R_c i_{c3} + V_3 + V_{Nm} \end{aligned} \quad (3.20)$$

or it can be written as:

$$v_{im} = L_c \frac{di_{ci}}{dt} + R_c i_{ci} + v_i + v_{Nm}, \quad where \;\; i = 1,2,3. \tag{3.21}$$

where v_{im} is the voltage between the midpoint of each inverter leg and the negative terminal of dc source, v_{Nm} is the voltage of the neutral point between negative DC terminal and ground, v_i is the load voltage or the voltage of the power grid, i_{ci} is the inverter current, $L_c \; and \; R_c$are the total inductance and resistance of the interface system and the transformer.

Assuming zero value component of the neutral current with the absence of the neutral wire, and with summing the equations in the eq.20, and assuming the system is also balance so that, $(V1 + V2 + V3 = 0)$, and $(ic1 + ic2 + ic3 = 0)$, the AC neutral point voltage equation is given by.

$$V_{Nm} = \frac{1}{3}\sum_{k=1}^{3} V_{km} \tag{3.22}$$

By rearranging the equations in (3.19), (3. 23) can be obtained as:

$$\begin{aligned}
\frac{di_{c1}}{dt} &= -\frac{R_C}{L_C} i_{c1} + \frac{V_{1m}}{L_C} - \frac{V_{Nm}}{L_C} - \frac{V1}{L_C} \\
\frac{di_{c2}}{dt} &= -\frac{R_C}{L_C} i_{c2} + \frac{V_{2m}}{L_C} - \frac{V_{Nm}}{L_C} - \frac{V2}{L_C} \\
\frac{di_{c3}}{dt} &= -\frac{R_C}{L_C} i_{c3} + \frac{V_{3m}}{L_C} - \frac{V_{Nm}}{L_C} - \frac{V3}{L_C}
\end{aligned} \tag{3.23}$$

The switching function of the legs of the VSI is defined by (3.24) as:

$$S_K = \begin{cases} 1, & if \; T_k \; is \; on \; and \; \overline{T_K} \; is \; off \\ 0, & if \; T_k \; is \; off \; and \; \overline{T_K} \; is \; on \end{cases} \tag{3.24}$$

By substituting $V_{Km} = S_K V_{dc}$ (where k= 1, 2 or 3) in (3. 24), (3.25) can be rewritten as:

$$\begin{aligned}
\frac{di_{c1}}{dt} &= -\frac{R_C}{L_C} i_{c1} + \frac{S_1}{L_C} V_{dc} - \frac{V_{Nm}}{L_C} - \frac{V1}{L_C} \\
\frac{di_{c2}}{dt} &= -\frac{R_C}{L_C} i_{c2} + \frac{S_2}{L_C} V_{dc} - \frac{V_{Nm}}{L_C} - \frac{V1}{L_C} \\
\frac{di_{c3}}{dt} &= -\frac{R_C}{L_C} i_{c3} + \frac{S_3}{L_C} V_{dc} - \frac{V_{Nm}}{L_C} - \frac{V1}{L_C}
\end{aligned} \tag{3.25}$$

In addition, by substituting the switching function in (3.21) and applying it in (3.25), the following equation is obtained [44]:

$$\begin{aligned}
\frac{di_{c1}}{dt} &= -\frac{R_C}{L_C} i_{c1} + \frac{1}{L_C}\left(S_1 - \frac{1}{3}\sum_{j=1}^{3} S_j\right) V_{dc} - \frac{V1}{L_C} \\
\frac{di_{c2}}{dt} &= -\frac{R_C}{L_C} i_{c2} + \frac{1}{L_C}\left(S_2 - \frac{1}{3}\sum_{j=1}^{3} S_j\right) V_{dc} - \frac{V2}{L_C} \\
\frac{di_{c3}}{dt} &= -\frac{R_C}{L_C} i_{c3} + \frac{1}{L_C}\left(S_3 - \frac{1}{3}\sum_{j=1}^{3} S_j\right) V_{dc} - \frac{V3}{L_C}
\end{aligned} \tag{3.26}$$

In addition, (3.27) below, represents the general equation of the proposed system:

$$\frac{dick}{dt} = -\frac{R_C}{L_C} ick + \frac{1}{L_C}\left(S_k - \frac{1}{3}\sum_{j=1}^{3} S_j\right) V_{dc} - \frac{Vk}{L_C} \quad where\ k = 1, 2\ or\ 3 \tag{3.27}$$

Equation (3.27) represents the k^{th} dynamic equation of the proposed model.

To simplify the dynamic system, the switching state function (d_{nk}), which describes all possible switching states of the VSI is defined as given in the (3.28) below.

$$d_{nk} = \left(S_K - \frac{1}{3}\sum_{J=1}^{3} S_j\right) \tag{3.28}$$

Equation (3.28) shows that, the value of the switching state function, d_{nk}, depends on the switching state "n" (on or off) in each phase "k" , so it describes the switching state function of the three leg VSI simultaneously, and describes the interaction between the three legs.

Based on (3.28) and for eight possibility of the switching function of the interfaced converter, (3.29) describes the conversion between [S_K] and [d_{nk}], as shown below [13].

$$\begin{bmatrix} d_{n1} \\ d_{n2} \\ d_{n3} \end{bmatrix} = \frac{1}{3} \begin{bmatrix} 2 & -1 & -1 \\ -1 & 2 & -1 \\ -1 & -1 & 2 \end{bmatrix} \begin{bmatrix} S_1 \\ S_2 \\ S_3 \end{bmatrix} \quad (3.29)$$

In addition, by substituting the (3.28) in (3.26), (3.30) can be expressed as:

$$\frac{dick}{dt} = -\frac{R}{L_C} ick + \frac{1}{L_C}\, d_{nk} V_{dc} - \frac{Vk}{L_C} \quad where\ k = 1, 2\ or\ 3 \quad (3.30)$$

The term $d_{nk} v_{dc}$ represent the output voltage of the inverter (v_{ck}). By substituting it in the (3.30) can be expressed as:

$$\frac{dick}{dt} = -\frac{R}{L_C} ick + \frac{1}{L_C}\, v_{ck} - \frac{Vk}{L_C} \quad where\ k = 1, 2\ or\ 3 \quad (3.31)$$

or

$$\frac{d}{dt} \begin{bmatrix} i_{c1} \\ i_{c2} \\ i_{c3} \end{bmatrix} = -\frac{R_C}{L_C} \begin{bmatrix} 1 & 0 & 0 \\ 0 & 1 & 0 \\ 0 & 0 & 1 \end{bmatrix} \begin{bmatrix} i_{c1} \\ i_{c2} \\ i_{c3} \end{bmatrix} + \frac{1}{L_C} \begin{bmatrix} v_{c1} \\ v_{c2} \\ v_{c3} \end{bmatrix} - \frac{1}{L_C} \begin{bmatrix} V_1 \\ V_2 \\ V_3 \end{bmatrix} \quad (3.32)$$

Furthermore, for the three-phase balanced system, ($i_{c1} + i_{c2} + i_{c3} = 0$) and ($V_1 + V_2 + V_3 = 0$), and based on (3.10), ($v_{c1} + v_{c2} + v_{c3} = 0$), so (3.32) can be rewritten as follows:

$$\frac{d}{dt} \begin{bmatrix} i_{c1} \\ i_{c2} \end{bmatrix} = -\frac{R_C}{L_C} \begin{bmatrix} 1 & 0 \\ 0 & 1 \end{bmatrix} \begin{bmatrix} i_{c1} \\ i_{c2} \end{bmatrix} + \frac{1}{L_C} \begin{bmatrix} v_{c1} \\ v_{c2} \end{bmatrix} - \frac{1}{L_C} \begin{bmatrix} V_1 \\ V_2 \end{bmatrix} \quad (3.33)$$

3.5.2 Transformation of The Dynamic Model Into d-q Orthogonal Frame

In order to simplify the control scheme, the general dynamic equation (3.31) can be transferred to the synchronous orthogonal rotating frame at the angular frequency (ω) of the system, so the positive sequence component at the fundamental frequency becomes constant, from which the fundamental frequency component and the harmonic components can be extracted.

To transform the dynamic equation to the d-q orthogonal frame, (3.34) and (3.35) must be apply to the dynamic equation of the system [13]:

$$\begin{bmatrix} V_1 \\ V_2 \\ V_3 \end{bmatrix} = \begin{bmatrix} \cos(\omega t) & -\sin(\omega t) & 1 \\ \cos\left(\omega t - \frac{2\pi}{3}\right) & -\sin\left(\omega t - \frac{2\pi}{3}\right) & 1 \\ \cos\left(\omega t + \frac{2\pi}{3}\right) & -\sin\left(\omega t + \frac{2\pi}{3}\right) & 1 \end{bmatrix} \begin{bmatrix} v_d \\ v_q \\ v_0 \end{bmatrix} = K \begin{bmatrix} v_d \\ v_q \\ v_0 \end{bmatrix} \quad (3.34)$$

$$\begin{bmatrix} v_d \\ v_q \\ v_0 \end{bmatrix} = K^{-1} \begin{bmatrix} v_1 \\ v_2 \\ v_3 \end{bmatrix} \quad (3.35)$$

where K represent the transformation matrix of (3.34).

From (3.32), the differential equation of the inverter, three phase injected currents can be transformed to the d-q frame using the (3.34) and (3.35). As shown below.

The dynamic equation of the interface system in (3.32) can be rewritten as follows:

$$-L_C \frac{d_{ik}}{dt} - R_C i_{ck} + d_{nk} V_{dc} = V_k \,, \; where \; k = 1, 2 \; or \; 3 \quad (3.36)$$

In addition, eq. 34 can be expressed as follows:

$$V_1 = v_d \cos(\omega t) - v_q \sin(\omega t) + v_0$$

$$V_2 = v_d \cos\left(\omega t - \frac{2\pi}{3}\right) - v_q \sin\left(\omega t - \frac{2\pi}{3}\right) + v_0 \quad (3.37)$$

$$V_3 = v_d \cos\left(\omega t + \frac{2\pi}{3}\right) - v_q \sin\left(\omega t + \frac{2\pi}{3}\right) + v_0$$

Substituting (3.36) in (3. 37) for each phase yield:

Phase 1:

$$-L_C \frac{d}{dt}\left[i_d \cos(\omega t) - i_q \sin(\omega t) + i_0\right] - R_C \left[i_d \cos(\omega t) - i_q \sin(\omega t) + i_0\right] +$$

$$[d_{nd} \cos(\omega t) - d_{nq} \sin(\omega t) + d_{n0}] v_{dc} = \left[v_d \cos(\omega t) - v_q \sin(\omega t) + v_0\right]$$

By differentiating and rearranging. The equations can be written as follows

$$-L_C[\frac{di_d}{dt}\cos(\omega t) - \omega i_d \sin(\omega t) - \frac{di_q}{dt}\sin(\omega t) - \omega i_q \cos(\omega t) + \frac{di_0}{dt}] - R_C[i_d \cos(\omega t) - i_q \sin(\omega t) + i_0] + [d_{nd}\cos(\omega t) - d_{nq}\sin(\omega t) + d_{n0}]v_{dc} = [v_d \cos(\omega t) - v_q \sin(\omega t) + v_0 \ ] \quad (3.38)$$

Phase 2:

$$-L_C \frac{d}{dt}\left[i_d \cos\left(\omega t - \frac{2\pi}{3}\right) - i_q \ \sin\left(\omega t - \frac{2\pi}{3}\right) + i_0\right] - R_C\left[i_d \cos\left(\omega t - \frac{2\pi}{3}\right) - i_q \sin\left(\omega t - \frac{2\pi}{3}\right) + i_0\right] + \left[d_{nd}\cos\left(\omega t - \frac{2\pi}{3}\right) - d_{nq}\sin\left(\omega t - \frac{2\pi}{3}\right) + d_{n0}\right]v_{dc} = \left[v_d \cos\left(\omega t - \frac{2\pi\pi}{3}\right) - v_q \sin\left(\omega t - \frac{2\pi}{3}\right) + v_0\right]$$

By differentiating and rearranging. The equations can be written as follows

$$-L_C[\frac{di_d}{dt}\cos\left(\omega t - \frac{2\pi}{3}\right) - \omega i_d \sin\left(\omega t - \frac{2\pi}{3}\right) - \frac{di_q}{dt}\sin\left(\omega t - \frac{2\pi}{3}\right) - \omega i_q \cos\left(\omega t - \frac{2\pi}{3}\right) + \frac{di_0}{dt}] - R_C[i_d \cos\left(\omega t - \frac{2\pi}{3}\right) - i_q \sin\left(\omega t - \frac{2\pi}{3}\right) + i_0] + [d_{nd}\cos\left(\omega t - \frac{2\pi}{3}\right) - d_{nq}\sin\left(\omega t - \frac{2\pi}{3}\right) + d_{n0}]v_{dc} = [v_d \cos\left(\omega t - \frac{2\pi}{3}\right) - v_q \sin\left(\omega t - \frac{2\pi}{3}\right) + v_0 \ ] \quad (3.39)$$

Phase 3:

$$-L_C \frac{d}{dt}\left[i_d \cos\left(\omega t + \frac{2\pi}{3}\right) - i_q \ \sin\left(\omega t + \frac{2\pi}{3}\right) + i_0\right] - R_C\left[i_d \cos\left(\omega t + \frac{2\pi}{3}\right) - i_q \sin\left(\omega t + \frac{2\pi}{3}\right) + i_0\right] + \left[d_{nd}\cos\left(\omega t + \frac{2\pi}{3}\right) - d_{nq}\sin\left(\omega t + \frac{2\pi}{3}\right) + d_{n0}\right]v_{dc} = \left[v_d \cos\left(\omega t + \frac{2\pi\pi}{3}\right) - v_q \sin\left(\omega t + \frac{2\pi}{3}\right) + v_0\right]$$

By differentiating and rearranging. The equations can be written as follows

$$-L_C[\frac{di_d}{dt}\cos\left(\omega t + \frac{2\pi}{3}\right) - \omega i_d \sin\left(\omega t + \frac{2\pi}{3}\right) - \frac{di_q}{dt}\sin\left(\omega t + \frac{2\pi}{3}\right) - \omega i_q \cos\left(\omega t + \frac{2\pi}{3}\right) + \frac{di_0}{dt}] - R_C[i_d \cos\left(\omega t + \frac{2\pi}{3}\right) - i_q \sin\left(\omega t + \frac{2\pi}{3}\right) + i_0] + [d_{nd}\cos\left(\omega t + \frac{2\pi}{3}\right) - d_{nq}\sin\left(\omega t + \frac{2\pi}{3}\right) + d_{n0}]v_{dc} = [v_d \cos\left(\omega t + \frac{2\pi}{3}\right) - v_q \sin\left(\omega t + \frac{2\pi}{3}\right) + v_0 \ ] \quad (3.40)$$

In addition, by summing the equations (3.38, 3.39 and 3.40) and rearranging, (3.41) can be written as follows:

$$\left[L_C \frac{di_{cd}}{dt} - L_C \omega i_{cq} + R_C i_{cd} - d_{nd} v_{dc} - v_d\right] \left[\cos(\omega t) + \cos\left(\omega t - \frac{2\pi}{3}\right) + \cos\left(\omega t + \frac{2\pi}{3}\right)\right] +$$

$$\left[L_C \frac{di_{cq}}{dt} + L_C \omega i_{cd} + R_C i_{cq} + d_{nq} v_{dc} - v_q\right] \left[\sin(\omega t) + \sin\left(\omega t - \frac{2\pi}{3}\right) + \sin\left(\omega t + \frac{2\pi}{3}\right)\right] +$$

$$3\left[L_C \frac{di_{c0}}{dt} + R_C i_{c0} + d_{n0} v_{dc} - v_0\right] = 0 \tag{3.41}$$

Therefore, from (3.41), the final dynamic equations of the proposed system in dq0 frame, and can be rewritten as follows:

$$\begin{aligned} L_C \frac{di_{cd}}{dt} + R_C i_{cd} &= \omega L_c i_{cq} - d_{nd} v_{dc} + v_d \\ L_C \frac{di_{cq}}{dt} + R_C i_{cq} &= -\omega L_c i_{cq} - d_{nq} v_{dc} + v_q \\ L_C \frac{di_{c0}}{dt} + R_C i_{c0} &= -d_{n0} v_{dc} + v_0 \end{aligned} \tag{3.42}$$

or can be written as follows:

$$\frac{d}{dt}\begin{bmatrix} i_{cd} \\ i_{cq} \\ i_{c0} \end{bmatrix} = \begin{bmatrix} -\frac{R_C}{L_C} & \omega & 0 \\ -\omega & -\frac{R_C}{L_C} & 0 \\ 0 & 0 & -\frac{R_C}{L_C} \end{bmatrix} \begin{bmatrix} i_{cd} \\ i_{cq} \\ i_{c0} \end{bmatrix} + \frac{1}{L} \begin{bmatrix} d_{nd} \\ d_{nq} \\ d_{n0} \end{bmatrix} v_{dc} - \frac{1}{L} \begin{bmatrix} v_d \\ v_q \\ v_0 \end{bmatrix} \tag{3.43}$$

For a three-phase balanced system, the homopolar value component is zero, so that ($i_0 = 0, v_0 = 0$), and furthermore for a balanced three-phase system ($v_1 + v_2 + v_3 = 0$) and ($i_{c1} + i_{c2} + i_{c3} = 0$), and based on eq. 29 ($d_{nd} + d_{nq} + d_{n0} = 0$), in addition by omitting the homopolar value, eq. 43 can be rewritten follows:

$$\frac{d}{dt}\begin{bmatrix} i_{cd} \\ i_{cq} \end{bmatrix} = \begin{bmatrix} -\frac{R_C}{L_C} & \omega \\ -\omega & -\frac{R_C}{L_C} \end{bmatrix} \begin{bmatrix} i_{cd} \\ i_{cq} \end{bmatrix} + \frac{1}{L_C} \begin{bmatrix} d_{nd} \\ d_{nq} \end{bmatrix} v_{dc} - \frac{1}{L_C} \begin{bmatrix} v_d \\ v_q \end{bmatrix} \tag{3.44}$$

3.6 Stationary Reference Frame Control in Three Phase Inverter System

The AC three phase inverter application and their controller have been studied with using the stationary reference frame transformation in detail in [45], [46]. The proportional resonant (PR) controller design is discussed a specific way in the recent published paper [47] , [48].

By using a current controller in the three-phase system, the three phase voltage source inverter (VSI) controller provide independent PWM source signal (three individual single phase sources). By implementation Clark transformation theory in the three phase system, the number of variable is reduced from three separate phase components to two orthogonal stationary reference frame. The two components are the primary key to implement the space vector pulse width modulation (SVPWM) technique instead of SPWM.

According to Clark transformation matrix (3.17), the phase angle is not important in this transformation. The control variable (voltage and current) in the stationary reference frame are time variant. Therefore, it is difficult to eliminate the steady state error by using the PI controller. Implementation of the proportional resonant controller (PR) has attracted considerable attention during the last decade. Equation (3.45) represents the transfer function of PR controller [46].

$$G_{P-R}^{\alpha\beta} = \begin{bmatrix} K_P + K_i \frac{s}{s^2+\omega^2} & 0 \\ 0 & K_P + K_i \frac{s}{s^2+\omega^2} \end{bmatrix} \tag{3.45}$$

where ω is the resonant frequency, K_P is the proportional gain, and K_i is the controller integral gain. The proportional resonant controller has a good performance, eliminating the steady state error of the sinusoidal signals, and has the ability to compensate the low order harmonics (harmonics compensator) as shown in (3.46) [48]:

$$G_{HC} = \sum_{h=3,5,7} K_i \frac{s}{s^2+(\omega.h)^2} \tag{3.46}$$

where h represents the harmonics order. The general block diagram structure of a controller using the proportional resonant controller with harmonics compensator is shown in Fig. 3.15.

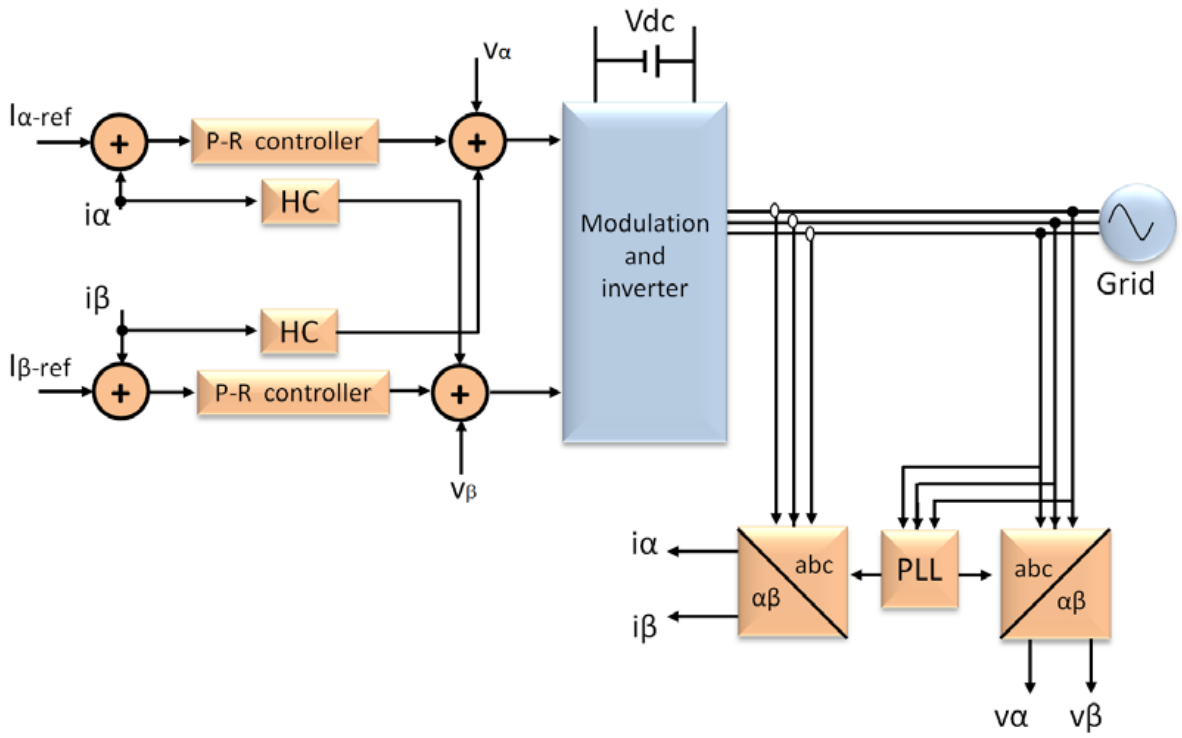

Fig. 3.15: General block diagram of the three phase PR control strategy

3.7 Rotating Reference Frame Control in The Three Phase Inverter System

By using the rotating reference frame method, another strategy for inverter control loop can be constructed. The rotating reference frame transformation theory (d-q transformation) is widely used in the controller of a three-phase industrial system. Rotating reference frame produces high performance in the current control of industrial system. Figure 3.16 shows the general block diagram of the d-q control strategy in a three phase inverter system [11], [49] and [50].

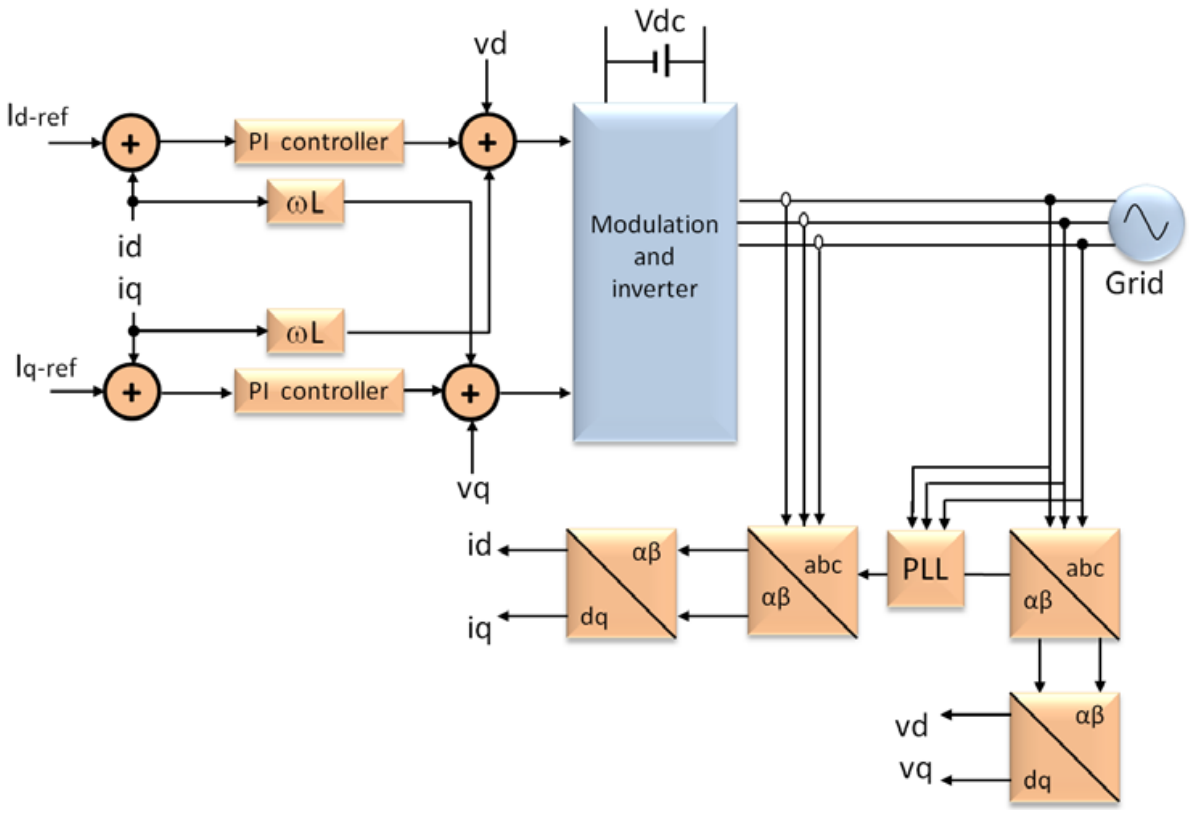

Fig. 3.16: General block diagram of a three phase rotating reference frame control strategy

According to the block diagram, the three phase measured current are transformed mathematically to two components (α, β) by applying the Clark transformation matrix in (3. 17), which are time variant system (stationary system). In the most industrial cases, three-phase system is balanced; therefore, three-phase voltages and currents are symmetrical, which means that the sum of the phase quantity becomes zero. By using the Park transformation matrix in (3.18), the stationary frame (α, β) is transformed to the synchronous rotating frame (d-q), the d-q quantity are rotating synchronously at the power line frequency.

The measured components of the currents in the stationary frame, transformed to the synchronous reference frame (d-q component), are compared with their reference values to

generate the feedback voltage in the synchronous reference frame that are fed to the compensator.

The active and reactive power (or voltage) contains a cross coupling and decoupling of the filter inductive term, caused by interaction between the inverter, filter circuit and PWM modulation scheme. The decoupling eliminate the coupling in the controller feedback signal between q and d channel to generate independent two current control loop. The reference voltage is added to the feedback reference signal to generate the d and q components of the reference voltage. To generate the switching signal to the gate of the semiconductor devices by using Sinusoidal Pulse Width Modulation technique (SPWM), it is necessary to transfer the d-q rotational frame to the stationary reference frame by using the inverse transformation of the Park and Clark matrix. Equation (3.47) represents the transfer function of the proportional integral controller in the rotating synchronous reference frame [31], [51], [41] and [49].

$$G_{PI}^{dq}(s) = \begin{bmatrix} K_P + \frac{K_i}{s} & 0 \\ 0 & K_P + \frac{K_i}{s} \end{bmatrix} \tag{3.47}$$

The major difference between the stationary and synchronous rotating reference frame current controller is that, most of stationary reference frame current controllers are inable to eliminate the steady state error. The problem is solved by using the synchronous rotating frame so it makes the fundamental power frequency represented as a DC quantity of the conventional DC regulator, such as PI controller can be used [10].

3.8 Virtual Synchronous Generator Structure

3.8.1 Overview

In this section, the theoretical concept and explanation of the synchronous generator in mechanical and electrical part are presented, which aid in the designing the virtual synchronous generator (VSG).

Figure 3.17 shows the cross section view of a single phase synchronous generator. The field coil of the generator is wound on the rotor while and the armature coils are wound on the stator. The rotor contains a damper coil, which has an effect on the transient operation of the generator.

The main features for producing a reliable and a stable operation of the electrical grid, are the rotor inertia in the synchronous generator, damping effect due to the damper windings, and speed droop characteristics of the synchronous generator [52].

Figure 3.18 shows the block diagram of the synchronous generator unit, which describe the control and behaviour of the complete unit [53].

The main control parts of the synchronous generator are:

1. Governor:

The function of the governor is to control the speed of the rotor (frequency of the generated voltage), or the output mechanical power according to the power-frequency characteristic of the machine.

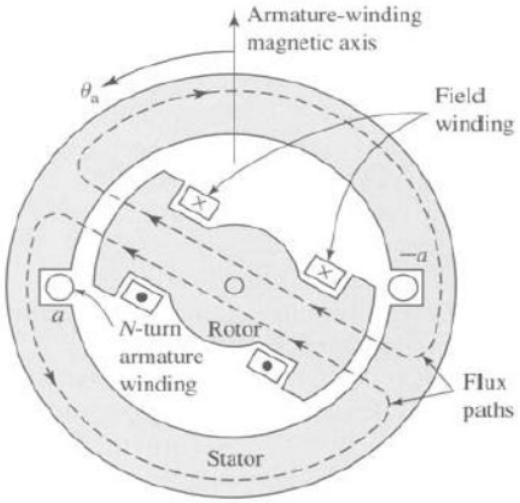

Fig. 3.17: The schematic view of single phase synchronous generator[52]

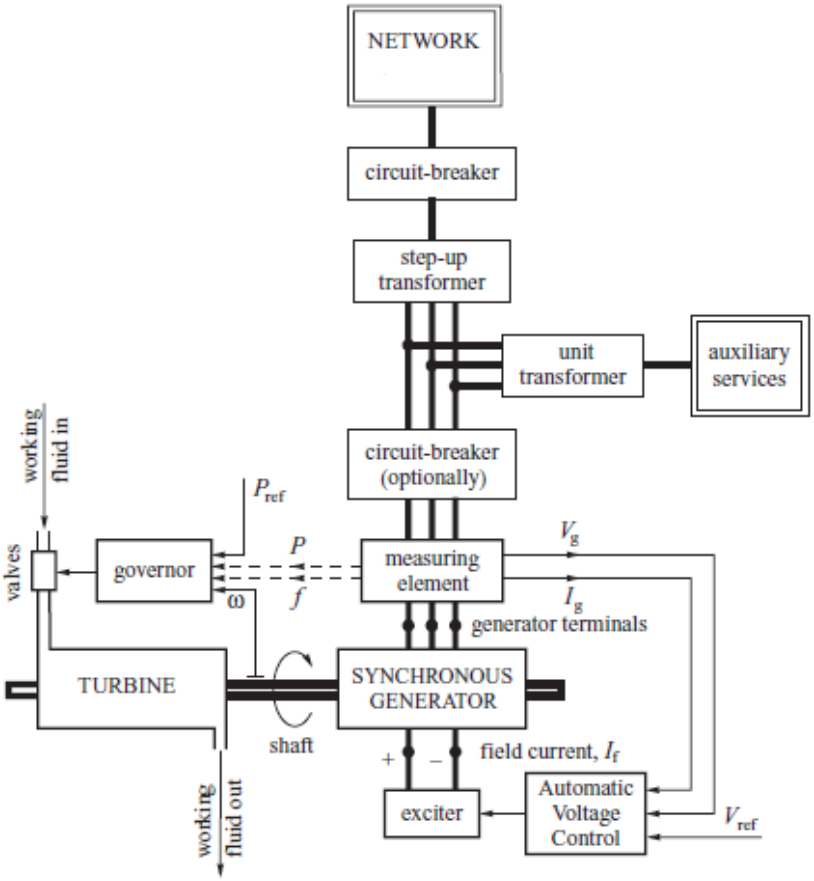

Fig. 3.18: The generation unit block diagram [54]

2. Automatic Voltage Regulator (AVR)

The function of the AVR is to control the voltage and reactive power supplied (or absorbed) by the generator.

3.8.2 Rotor Inertia in the Synchronous Generator

When the rotor with a field and damper winding rotates, it will create a sinusoidal flux in the air gap, which produces voltages in the stator windings.

The swing equation of the synchronous generator dynamics is given by [17]:

$$J\frac{d\omega}{dt} = \tau_m - \tau_e - B\Delta\omega \,, where\ \Delta\omega = \omega - \omega_{syn} \quad (3.48)$$

where:

J : Moment of inertia of the rotor

τ_m : Mechanical torque

τ_e : Electromagnetic torque

B : Damping torque coefficient

ω : Angular speed of the rotor shaft

ω_{syn}: Synchronous speed

Under steady state condition:

$$\omega = \omega_{syn} = const$$

$$\therefore B\Delta\omega = 0 \ \& \ \tau_m = \tau_e$$

The mechanical torque (τ_m) has a higher time constant due to the slow torque response in the prime mover. Hence, the changes are relatively slow, upon an imbalance in the electrical

network. The electromagnetic torque (τ_e) can be varied almost instantaneously. Therefore due to some disturbances, if $\tau_e < \tau_m$, the rotor will accelerate and if $\tau_e > \tau_m$ the rotor will be deaccelerated.

3.8.3 Damper Windings Effect

The damper coil introduces the damping effect in the synchronous generators, which maintains the synchronism of the generator when a deviation in the rotor's speed occurs due to disturbances.

From the swing equation, the power equation is given by [53]:

$$J\omega \frac{d\omega}{dt} = P_m - P_e - P_D\,, \quad wher\ P_D = B\Delta\omega \tag{3.49}$$

Fig. 3.19 shows the oscillation of the Rotor and power under the effect of damping when a small disturbance occurred.

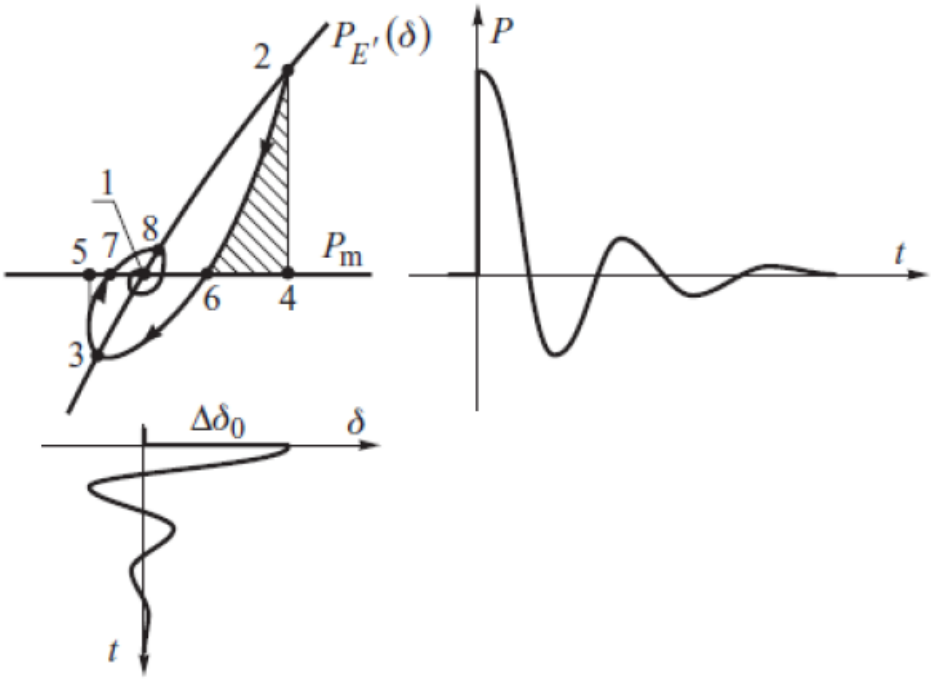

Fig. 3.19: The Rotor and power oscillations with damping effect included[53]

If the rotor is deviated from the equilibrium point due to the disturbance, it will accelerate or decelerate. According to the swing equation, if $\Delta\omega$ >zero, damping power will be negative and if the $\Delta\omega$<zero, damping power will be positive effect, and supporting the air gap power P_e. Therefore, the rotor speed will change instantaneously and to reach the synchronous speed without any vibration or infinite oscillation [53].

3.8.4 Droop Characteristics of Synchronous Generator

This section gives more explanation of the advantage of the inertia in SG due to its rotating mass of the rotor. The advantage will be noticed in the active power or load-sharing characteristic between two generators working in islanded system.

According to the swing equation, it is clear that when there is a mismatch between the input mechanical power supplied by the prime mover and the output electrical power supplied by the generator to the grid, the rotor speed will deviate from the synchronous speed.

The speed load dependence of two parallel synchronous generators can be characterized by the housing diagram, which is shown in Fig. 3.20 [52],[54].

When two generator are adjusted to operate in parallel, they will work at the same frequency. If the load increase, the additional load will be shared by the two generators according to their drop characteristic. However, if the frequency decreases below the threshold value, the reference speed of the governor for both SGs needs to be readjusted.

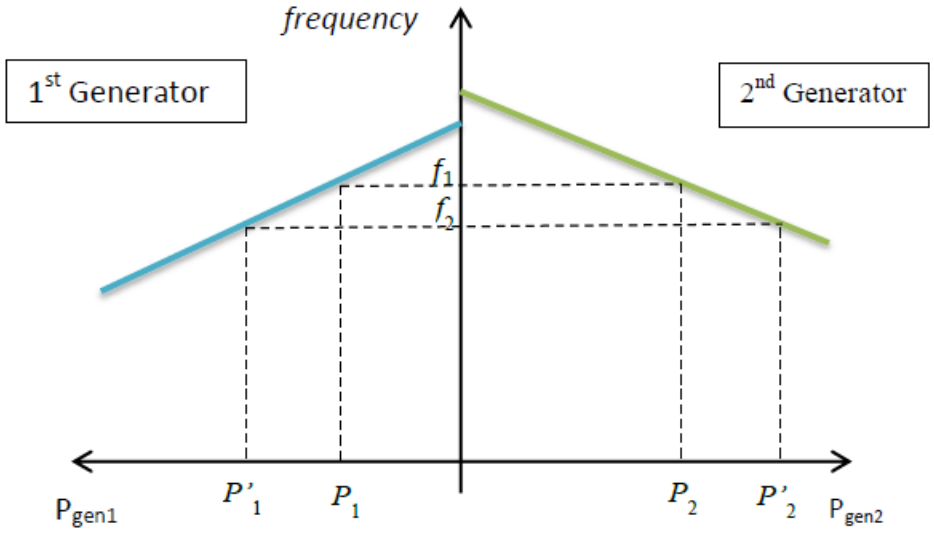

Fig. 3.20: The speed-droop characteristics of two synchronous generator [52]

The frequency of the terminal voltage of the synchronous generator is related to mechanical speed and number of poles as [52]:

$$f_e = \left(\frac{pole}{2}\right) * \frac{n}{60} \tag{3.50}$$

Chapter 4

Control System of The Inverter

The control system of the inverter is responsible to control the current performance of the Voltage Source Inverter (VSI) based on analyses of the voltage and current vector in the stationary and rotating frames. The voltage and current vector are transferred from abc to αβ and from αβ to dq, by using park and clack transformation matrices. By using these transformation matrices, it is easy to control of the current and voltage because the current and voltage is converted to a constant value. In this way, it is easy to extract the harmonics and the fundamental value of the current from the AC current signal. By using this technique, a flexible distribution generator with the following characteristics can be achieved:

- Compensation of harmonic currents (active filter)
- Compensation of load reactive power (DSTATCOM)
- Control of active power with proper stability and damping during disturbances (VSG)

4.1 Voltage and Current in the α-β and d-q Reference Frame

The control technique used in the proposed system is based on analysing the voltage and current vector component in the αβ and dq reference frame, including the mathematical equation, and transformation matrix. The Clark transformation transfers the instantaneous three-phase current and voltage in abc system into instantaneous voltage and current in αβ-axes, and after that they are transferred from the αβ components into the dq reference frame, by using Park transformation, to transfer it to the rotating frame, which rotates at the angular

velocity (ω) of the grid frequency. In this frame, the voltage and current components represent as constant value. Therefore, it is easy to filter it to extract the fundamental and the harmonic components and it is easy to control of the current and voltage of the interface system. To calculate the voltage and current component in the dq reference frame, the instantaneous angle must be calculated. A Phase Locked Loop (PLL) is commonly used to obtain this angle in the vector control loop.

Fig 4.1 shows the voltage and current components in the dq and αβ reference frame, by considering the voltage vector in the d-axis vector direction. With this consideration, the q-component of the voltage vector in the dq rotating reference frame will be equal to zero ($v_q = 0$). By referring to Fig 4.1, the instantaneous angle of the grid voltage can be calculate as shown in (4.1).

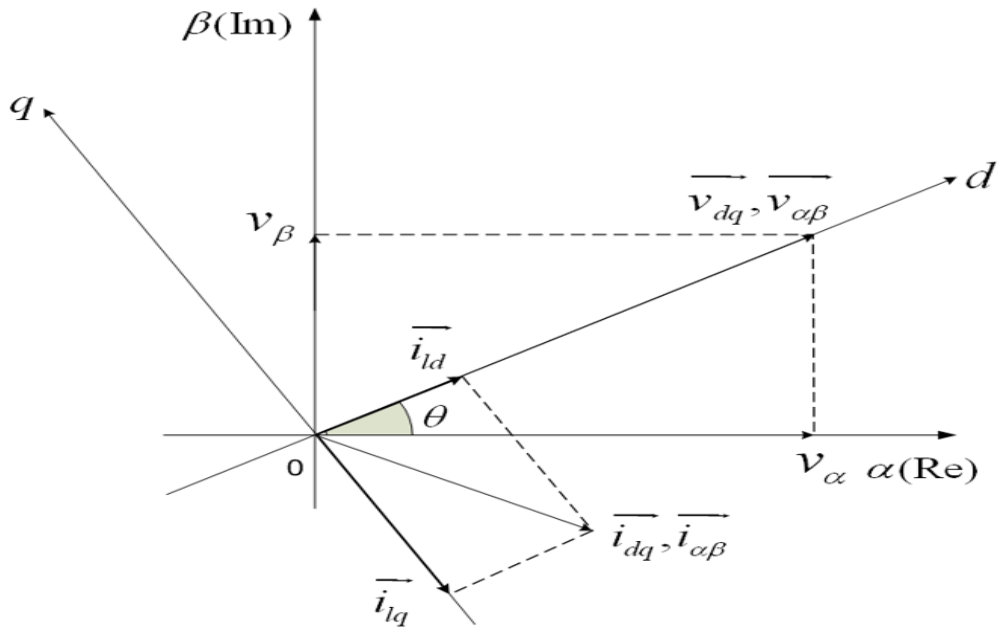

Fig. 4.1: The voltage and current component in the dq and α – β frames

$$\theta = \tan^{-1}\left(\frac{v_\beta}{v_\alpha}\right) \tag{4.1}$$

where θ is transformation angle.

Under balanced voltages of the main source, θ increases as a function of time uniformly, and the transformation angle θ is sensitive to the voltage components including the harmonics and unbalanced voltages, so that ω may be constant over the main period.

In addition, by considering the voltage in the direction of the d-axis, the reference voltage of the system at the point of the common coupling will be the load voltage, which can be expressed as:

$$v_{ref} = \left|\overrightarrow{v_{dq}}\right| = \left|\overrightarrow{v_d}\right| = \left|\overrightarrow{v_{\alpha\beta}}\right| = \left|\sqrt{v_\alpha^2 + v_\beta^2}\right| \tag{4.2}$$

The dq load current components (i_{ld}, i_{lq}) are delivered for the synchronous frame based on the Park transformation as shown in (4.3). They represent the active and reactive components of the load current respectively, so from the geometric relationship in the eq.3 the reference load current can be written as follows:

$$\begin{bmatrix} i_{ld} \\ i_{iq} \end{bmatrix} = \frac{1}{\sqrt{v_\alpha^2 + v_\beta^2}} \begin{bmatrix} v_\alpha & v_\beta \\ -v_\alpha & v_\beta \end{bmatrix} \begin{bmatrix} i_{l\alpha} \\ i_{l\beta} \end{bmatrix} \tag{4.3}$$

The instantaneous active and reactive load currents are constructed from the oscillatory components (harmonic components) and the average term (fundamental component).

$$i_{ld} = \widetilde{i_{ld}} + I_{ld} \;\; and \; i_{lq} = \widetilde{i_{lq}} + I_{lq} \tag{4.4}$$

The first term in the both equations $\widetilde{i_{ld}}$ & $\widetilde{i_{lq}}$ represents the high order harmonics current with the first harmonic of negative sequence, which is a non-dc quantity, and has oscillatory components, whilst the second term represents the first order harmonic frequency, which represents the current at the fundamental frequency (average value), and has a constant value (dc value).

The main advantage of this method is that, θ can be calculated directly from the main voltage source at the PCC, which avoids direct using of the PLL in the control circuits, therefore the large problem of synchronizing can be avoided.

4.2 Calculation of The Reference Current for DG Proposed System

4.2.1 Reference Current to Supply the Load Active Power

At the fundamental frequency the active power injected to the grid from the DG is given by (4. 5) as follow [13]:

$$P = \frac{3}{2}\left(v_d I_{cd} + v_q I_{cq}\right) \tag{4.5}$$

From (4.5), the capital letter related to the current injection by the DG at the fundamental frequency, and by referring to the first assumption ($v_q = 0$), and the reference voltage at the PCC is calculated in (4.2). The d-component of the reference current providing the active power at the fundamental frequency can be written as follows.

$$I_{cd}^{*} = \frac{2}{3}\,\frac{P_{ref}}{v_d} \tag{4.6}$$

where p_{ref} is the maximum power that the VSI can deliver to the network at the fundamental frequency, and I_{cd}^{*} represents the d-component of the DG reference current at fundamental frequency.

From this method, the active current is limited and restricted to the rated power of the VSI, and can control the maximum active power injection by the converter to the grid.

The reference active power depends on the DG system capacity, ratings of the power electronic converter, and the interface transformer.

4.2.2 Harmonic Components of the d-axis Reference Current.

In the dq reference frame, the fundamental component of the load current is seen, as a dc component value, and the harmonic components are oscillatory components. To extract the harmonic components from the load current in the d-axis, high pass filter (HPF) can be used. With a digital implementation of the control system, and by using this method, a delay occurs in the control system [8]. Thus, to avoid this problem, a minimal phase HPF can be obtained (MPHPF), by using a low bass filter to extract the dc component and to subtract it from the load current in the d-axis, which can be represented by:

$$H_{MPHPF}(s) = I_l(s) - H_{LPF}(s) \tag{4.7}$$

where $I_l(s)$ is the total load current.

The transfer function of this LPF is the same order and cut-off frequency of the HPF. A first order LPF is used in this proposed system with a cut-off frequency ($f_c = f/2$, where f = 50Hz) to extract the dc component from the nonlinear load current.

The overall load current in the d-axis is given by (4.8). To make the DG work as an active power filter all the harmonics component of the nonlinear load we must be supplied. Alternative part component of the load current is extract using the MPHPF. The dc-part is given by (4.6). Therefore, the reference current in the d-axis component is given by the relationship:

$$i_{cd}^{*} = \widetilde{i_{ld}} + I_{cd}^{*} \tag{4.8}$$

where:

i_{cd}^{*} : is the reference current to supply the load reactive power

$\widetilde{i_{ld}}$: is the harmonics component of the load reactive power

I_{cd}^{*} : is the load reactive current at the fundamental frequency

4.2.3 Reference Current to Supply The Load Reactive Power

In the d-q rotating reference frame, the quadrature component of the load current is perpendicular to the direct component of the voltage ($v_d \perp i_{lq}$) [49]. The reactive power of the load is represented by the q-component of the load current. To make the DG work as a reactive power compensator, the DG must inject all the current in the q-axis with both dc and alternating value.

For this purpose and to make the inverter work as a DG unit, it is sufficient to set the reference current of the inverter to the q-component of the load current as shown in the equation below.

$$i_{cq}^{*} = i_{lq} \tag{4.9}$$

For this consideration, the load reactive power will be compensated by the DG link in both components (harmonics and fundamental parts).

4.3 Steady State Analysis

By using the park transformation matrix, the dynamic model of the proposed system is transferred into the dq reference frame. By neglecting the homoplar value component of the voltage and current, all the Park Transformation variable of the DG become constant in the steady state condition, and the reference current is generated from the instantaneous active and reactive power of the nonlinear load.

By considering, the three-phase voltage to be balanced. The sum of the currents is zero. Therefore, no homopolar component ($i_{c0} = 0$). The voltage at the neutral point does not effect, any transformed current, and this voltage is given as follows:

$$v_{NM} = \frac{v_0 - v_{0M}}{\sqrt{3}} \tag{4.10}$$

where v_0 represents the homopolar component of the grid voltage, and v_{oM} represents the homopolar component of the of the voltage of the converter. The voltage at the neutral point depends on the homopolar component of the grid and the converter voltage. When the voltages of the power grid are balanced, the average value of the v_0 is zero. Therefore, the voltage v_{NM} depends on the homopolar value of the voltage of the interface converter.

By considering the original position of the load voltage on the d-axis, the voltage vector in the q-axis is equal zero ($v_q = 0$), so that the voltage vector is the d-component of the load voltage vector, which is equal the line-to-line rms voltage of the grid voltage (v_d). Equations (3.44) can be rewritten as follow.

$$\frac{d}{dt}\begin{bmatrix} i_{cd} \\ i_{cq} \end{bmatrix} = \begin{bmatrix} -\frac{R_C}{L_C} & \omega \\ -\omega & -\frac{R_C}{L_C} \end{bmatrix}\begin{bmatrix} i_{cd} \\ i_{cq} \end{bmatrix} - \frac{1}{L_C}\begin{bmatrix} v_{cd} \\ v_{cq} \end{bmatrix} + \frac{1}{L_C}\begin{bmatrix} v_d \\ 0 \end{bmatrix} \tag{4.11}$$

4.3.1 Current Control Technique for The Proposed Model

To eliminate the steady state error and to obtain low overshoot, and high accuracy, of the load current, a PI-controller is used to control the compensator current instead of the complex controller, and to provide the active and the harmonic components of the current.

The control strategy of the current control loop is based on the dynamic equation in the dq reference frame (4.11). As mentioned before, all the transformation variable in the dq frame become constant value in the steady state condition. The equation will be controlled in two different ways. The differential equation that represents the dynamic response of the system is shown in (4.12), and (4.13), as follow:

$$L_c \frac{di_{cd}}{dt} + R_c i_{cd} - \omega L_c i_{cq} - v_{cd} + v_d = 0 \quad (4.12)$$

$$L_c \frac{di_{cq}}{dt} + R_c i_{cq} + \omega L_c i_{cd} - v_{cq} = 0 \quad (4.13)$$

Based on (4.12) and (4.13), the equivalent circuit of the proposed model is drawn as shown in Fig. 4.2.

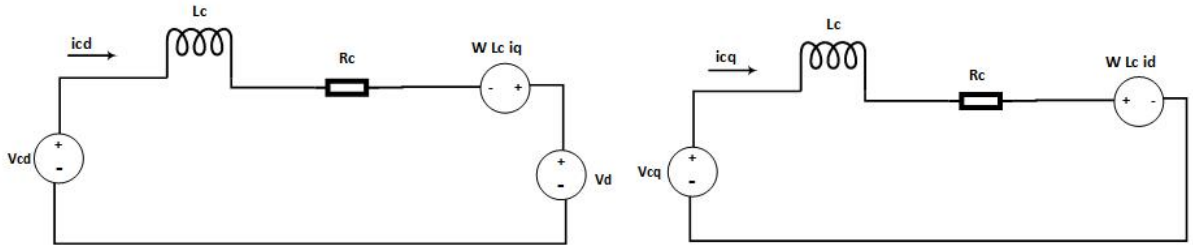

Fig. 4.2: The Equivalent circuit of the proposed model in d and q frame

In the figure, the V_{cdq} represents the output voltage of the voltage source inverter (VSI) when it's working as DG unit. $L_c \frac{di_{cd}}{dt} + R_c i_{cd}$ and $L_c \frac{di_{cq}}{dt} + R_c i_{cq}$ represents the output signal of the plant on the d-axis and q-axis respectively. By considering $\lambda_d = L_c \frac{di_{cd}}{dt} + R_c i_{cd}$ and $\lambda_q = L_c \frac{di_{cq}}{dt} + R_c i_{cq}$, the switching state function (v_{cd} , v_{cq}), is calculated as follows:

$$v_{cd} = \lambda_d - \omega L_c i_q + v_d \quad (4.14)$$

$$v_{cq} = \lambda_q + \omega L_c i_d \quad (4.15)$$

The two control loops consist of combination of a nonlinearity cancelation part and a linear compensation part, and a block containing L_C ω, whose objective is to decouple the influence between both current control loops in d-axis and q-axis.

Designing a PI controller for the two separate control loop can be derived from the λ_d and λ_q, as mentioned before. Taking the Laplace transform of the two equations yields.

$$\lambda_d(s) = L_c s I_{cd}(s) + R_c I_{cd}(s)$$

$$\lambda_q(s) = L_c s I_{cq}(s) + R_c I_{cq}(s)$$

The transfer functions are given as:

$$\frac{I_{cd}(s)}{\lambda_d(s)} = \frac{1}{L_c s + R_c} \tag{4.16}$$

$$\frac{I_{cq}(s)}{\lambda_q(s)} = \frac{1}{L_c s + R_c} \tag{4.17}$$

The parameter of the PI controller can be obtained as follow:

$$\lambda_{cd} = k_p \Delta i_{cd} + k_i \int (\Delta i_{cd}) dt \tag{4.18}$$

$$\lambda_{cq} = k_p \Delta i_{cq} + k_i \int (\Delta i_{cq}) dt \tag{4.19}$$

where k_p and k_i are the proportional and integral gains. $\Delta i_{cd} = i_{cd}^* - i_{cd}$ and $\Delta i_{cq} = i_{cq}^* - i_{cq}$, are the error signals that control the switching signals of the converter, according to the objective of the interconnection of the DG to the power grid.

The transfer function of the PI controller is obtained by tacking the Laplace transform of (4.18) and (4.19) yields:

$$\frac{\lambda_d(s)}{\Delta I_d(s)} = \frac{\lambda_q(s)}{\Delta I_q(s)} = k_p + \frac{k_i}{s} = \frac{k_p s + k_i}{s} \tag{4.20}$$

The block contains ωL_c is presented the both two current loops in the d and q axes. The original control inputs D_{nd} and D_{nq} consist of a non-linearity cancellation part and a linear decoupling compensation part. To achieve a fast dynamic response and a zero steady state error especially, when a nonlinear load or an unbalanced load is connected to the grid, a PI controller type is required. The closed loop control system is shown in the Fig. 4.3.

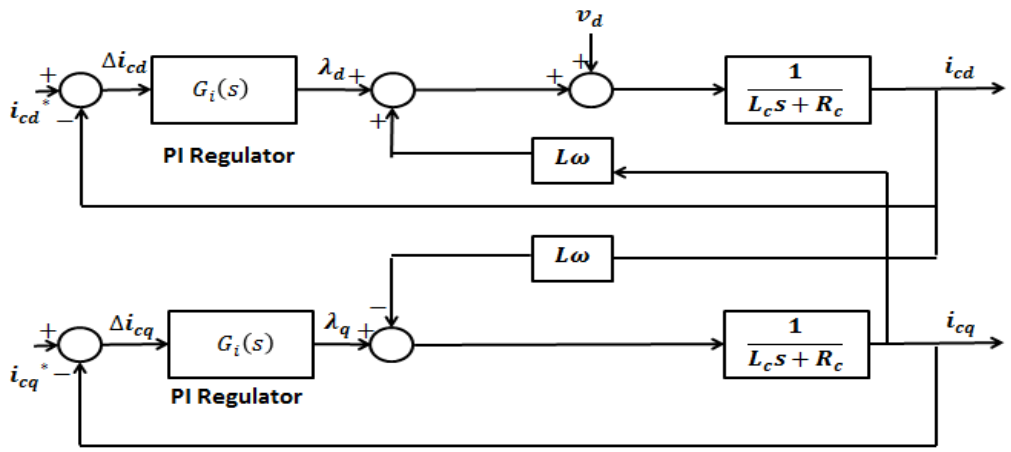

Fig. 4.3: The vector control loop in the d and q plane with PI regulator

To design the PI regulator of the current controller, it is necessary to decouple the proposed model by adding the measured voltage of the d-axis and cross-coupling terms as shown in Fig. 4.3. The block diagram of the current controller can be simplified as shown in Fig. 4.4.

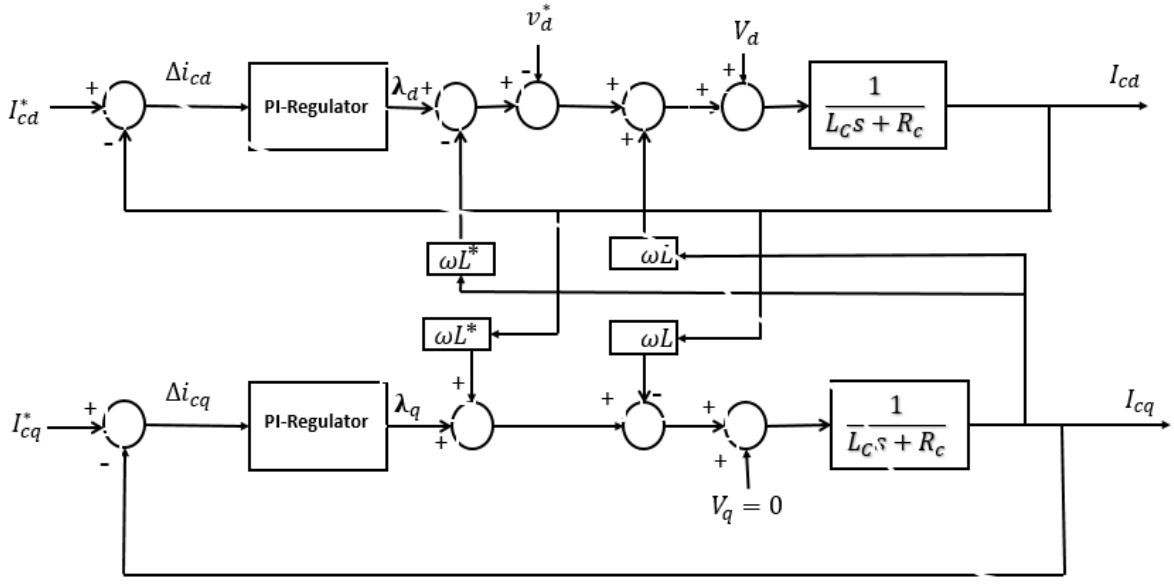

Fig. 4.4: The control block diagram of the current control loop in d and q axis

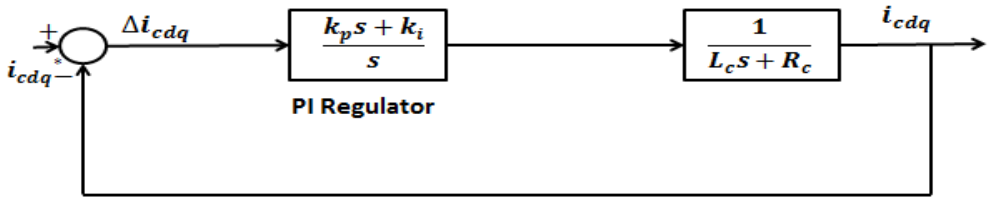

Fig. 4.5: The Equivalent block diagram of the current control loop in dq-axis

The closed loop transfer function of the current controller is given by:

$$\frac{I_{cd}(s)}{I_{cd}^*(s)} = \frac{I_{cq}(s)}{I_{cq}^*(s)} = \frac{k_p}{L_c} \frac{s+\frac{k_i}{k_p}}{s^2+\frac{(R_c+k_p)}{L_c}s+\frac{k_i}{L_c}} \tag{4.21}$$

The transient response of the control system will be effected by the presence of zero at $s = -\frac{k_i}{k_p}$. The presence of the zero in the control system produces high overshoot in the transient; when apply it on the Matlab program the theoretical overshoot is 20.79 % is noticed, which is high value. To eliminate the zero in the control system a pre-filter is added to the control system as shown in the Fig. 4.6, whose transfer function is [45]:

$$G_p(s) = \frac{1}{s+\frac{k_i}{kp}} \tag{4.22}$$

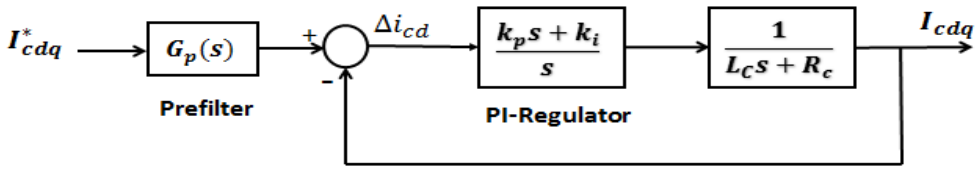

Fig. 4.6: The equivalent control block diagram in the d and q axis after adding pre-filter to eliminate the presence of the zero in the system

In this case, the transfer function will be given by:

$$F(s) = \frac{k_p}{k_i} \frac{\frac{k_i}{L_c}}{s^2 + \left(\frac{R_c + k_p}{L_c}\right)s + \frac{k_i}{L_c}} \tag{4.23}$$

$$F(s) = \frac{\omega_n^2}{s^2 + 2\zeta\omega_n s + \omega_n^2} \tag{4.24}$$

where ζ is the damping factor and ω_n is natural undamped angular frequency, which is dependent on the specific time response. Because of the physical limitation, ω_n must be lower than the angular frequency ω ($\omega = 2\pi f$, where f = 20 kHz) of the modulation carrier wave, which represents the switching frequency of the semiconductor devices. The value of $\omega_n = \omega/5$ based on the theorem of Shannon-Nyquist [55],[56], and the optimal value of the damping factor $\zeta = \sqrt{\frac{1}{2}}$. Equating (4.23) and (4.24) yields:

$$k_p = 2L_C\zeta\omega_n - R_C\,, \qquad K_i = L_C\omega_n^2 \tag{4.25}$$

4.3.2 DC-Bus Voltage Regulation

The differential equation of the inverter DC side is given by [55]:

$$\frac{dv_{dc}}{dt} = \frac{1}{c_{dc}} i_{dc} \tag{4.26}$$

where i_{dc} is equal to the AC output current of the inverter. By assuming an ideal condition, (4.26) can be rewritten as follows:

$$\frac{dv_{dc}}{dt} = \frac{1}{c_{dc}} \sum_{k=1}^{3} d_{nk} i_{ck} \tag{4.27}$$

where d_{nk} is the gate signal in the transistor number n in the phase number k.

By transforming the parameter into the dq reference frame, the dynamic equation in the dc-side bus is rewritten as:

$$\frac{dv_{dc}}{dt} = \frac{1}{c_{dc}} d_{nd} i_{cd} + \frac{1}{c_{dc}} d_{nq} i_{cq} \tag{4.28}$$

The transfer function of the plant can be obtained by taking the Laplace transform of (4.26) as follows.

$$\frac{V_{dc}(s)}{I_{dc}(s)} = \frac{1}{sc_{dc}} \tag{4.29}$$

The overall control block diagram is shown in the Fig. 4.7, where the error signal of the dc-bus voltage ($\Delta v_{dc} = v_{dc}^{*} - v_{dc}$) is passed through the PI-controller to regulate the voltage across the dc bus (v_{dc}) at a fixed value. Therefore, u_{dc} will be obtained as follows:

$$u_{dc} = k_1 \Delta v_{dc} + k_2 \int \Delta v_{dc} dt \tag{4.30}$$

where k_1 and k_2 are the proportional and integral gains. The closed loop transfer function of the overall control system is obtained as follows.

$$\frac{V_{dc}(s)}{V_{dc}^{*}(s)} = \frac{k_1}{c} \frac{s+\frac{k_2}{k_1}}{s^2+\frac{k_1}{c}s+\frac{k_2}{c}} \tag{4.31}$$

By comparing the transfer function with the general formula of the second order transfer function, which is given by:

$$F(s) = 2\zeta\omega_n \frac{s+\frac{\omega_n}{2\zeta}}{s^2+2\zeta\omega_n s+\omega_n^2} \tag{4.32}$$

The proportional and integral gains are obtained as follows.

$$k_1 = 2\zeta\omega_n c \qquad k_2 = \omega_n^2 c$$

By referring to the control loop, which is shown in Fig. 4.7, the control effort is obtained as:

$$i_{do}^{*} = \frac{u_{dc} - D_{nq}}{D_{nd}} = \frac{u_{dc} v_{dc} - D_{nq} v_{dc} i_q}{D_{nd} v_{dc}} \tag{4.33}$$

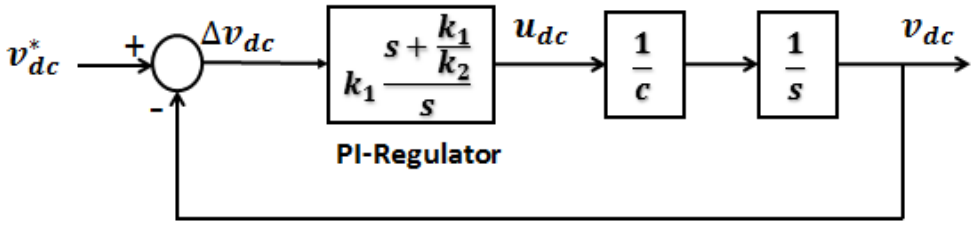

Fig. 4.7: The control block diagram of the dc-bus voltage

Therefore, by referring to the normal operation of the VSI as a DG unit, and assuming the ideal conditions for the current control loop, the following properties will be obtained:

$$D_{nd} v_{dc} \approx v_d \qquad D_{nq} v_{dc} \approx v_q$$

By assuming a balanced three phase grid voltages:

$$V_1 = v \cos(\omega t)$$

$$V_2 = v \cos\left(\omega t - \frac{2\pi}{3}\right) \tag{4.34}$$

$$V_3 = v \cos\left(\omega t + \frac{2\pi}{3}\right)$$

Transforming the voltages into the synchronous reference frame yields:

$$\begin{bmatrix} V_d \\ V_q \end{bmatrix} = T_{dq} \begin{bmatrix} V_1 \\ V_2 \end{bmatrix} = \sqrt{\frac{3}{2}} \begin{bmatrix} v \\ 0 \end{bmatrix}$$

By referring to the first assumption, we get

$$D_{nd} v_{dc} = v_d = \sqrt{\frac{3}{2}} v$$

$$D_{nq} v_{dc} = v_q = 0$$

Hence, the control effort can be approximate by:

$$i_{d1h+} \approx \sqrt{\frac{2}{3}}\frac{v_{dc}}{v}u_{dc} \tag{4.35}$$

where i_{d1h+} represents the first harmonics current of the positive sequence after converting it to the dc-quantity, so it is added to the reference current of the loop of i_{ld} to generate the current at the fundamental frequency. Furthermore, the dc voltage loop is designed to be much slower than the current one, to avoid any interaction between the two loops [13].

4.3.3 Virtual Inertia and Virtual Damping

A virtual Synchronous Generator (VSG) model has been developed using the swing equation (3.49). Based on the swing equation ($P_m - P_e - P_D = J\omega\frac{d\omega}{dt}$), the following deduction can be expressed to elaborate how the phase angle of the VSG is calculated:

$$\int \frac{2}{J}(P_m - P_e - P_D)dt = \int 2\omega\frac{d\omega}{dt}$$

$$\therefore \quad \frac{2}{J}\int (P_m - P_e - P_D)dt = \omega^2 \tag{4.36}$$

By further integration:

$$\int \sqrt{\omega^2}dt = \theta_{VSG} \tag{4.37}$$

The active power droop control has also been executed in this model based on the following relationship:

$$P_m = P_{ref} + \frac{f_{ref} - f_{VSG}}{droop}\ , droop > 0 \tag{4.38}$$

In addition, the virtual damping has been implemented based on the following relationship to represent the round rotor synchronous generator behaviour [52]:

$$P_D = K_{damping} * \left(\omega_{VSG} - \omega_{grid}\right) \tag{4.39}$$

By converting the model into the dq rotating frame, the reference and electrical power are given by:

$$P_{ref} = \frac{3}{2} v_d I_d^* \tag{4.40}$$

$$P_e = \frac{3}{2} v_d I_{cd} \tag{4.41}$$

Figure 4.8 shows the general block diagram for inertia and damping power emulation to generate the angle and frequency of the DG unit.

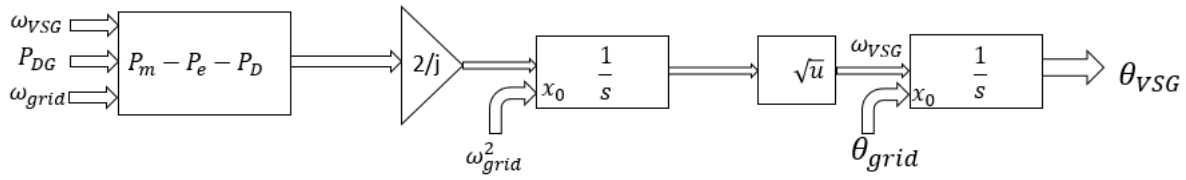

Fig. 4.8: The inertial structure with mechanical dynamic

The overall control system is shown in the Fig. 4.9, which is simulated using matlab/Simulink environment, and the capability of the control system is explained in the simulation section.

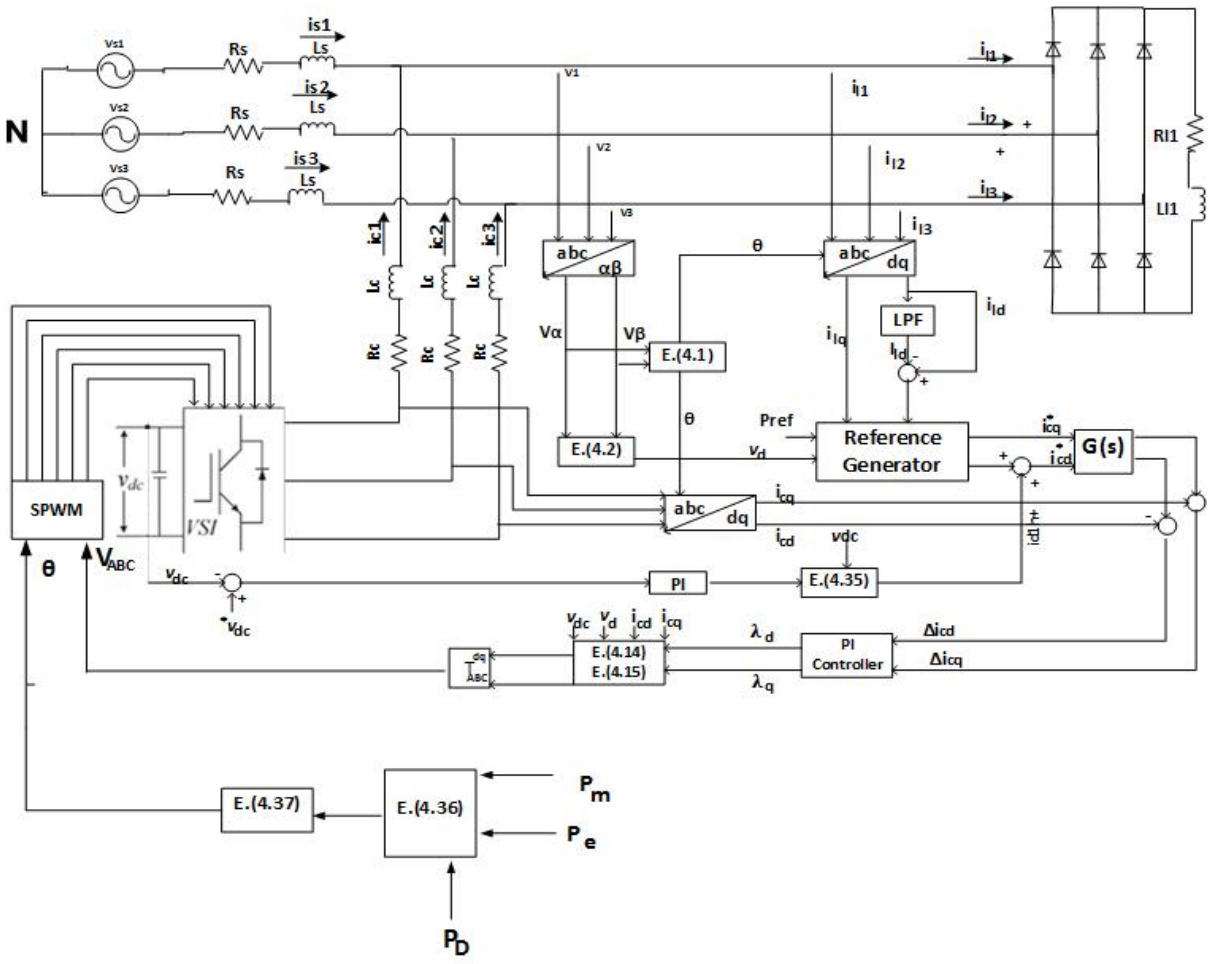

Fig. 4.9: The general schematic diagram of the control strategy for the DG system

4.4 Capability Curve of The DG Unit.

The dynamic state equations that represent the AC and the DC subsystem are presented using (3.30) and (4.28), which can be transferred to the dq reference frame by using the park transformation matrix. According to the general state space equation, the general proposed model can be expressed using (3.44), and (4.28).

By referring to the first assumption, the direction of the reference vector of the grid voltage in phase with the d-axis, and the q-component of the grid voltage is equal to zero ($v_q = 0$), the reference voltage is equal to the d-component of the grid voltage ($v_d = v_m$). Assuming that,

the reference value of the d-axis in the current control loop in the DG unit to inject the appropriate reactive power is equal to I_{refd} ($I_{cd} = I_{refd}$), I_{refq} represents the reference current to provide the reactive power to the load, and v_r is the desired value of the dc voltage ($v_{dc} = v_r$).

By considering the stability criteria in the proposed model and substituting these assumptions given in (3.44) and (4.28), and considering d_{nd} and d_{nq} are the switching values during the steady state operation condition, a set of equations can be obtained during the steady state condition of the proposed model as follows:

$$L_c \frac{dI_{refd}}{dt} + R_c I_{refd} - \omega L_c I_{refq} + d_{nd} v_r + v_m = 0 \tag{4.42}$$

$$L_c \frac{dI_{refq}}{dt} + R_c I_{refq} + \omega L_c I_{refd} + d_{nq} v_r = 0 \tag{4.43}$$

$$d_{nd} I_{refd} + d_{nq} I_{refq} + I_{dc} = 0 \tag{4.44}$$

In order to meet the appropriate compensation during the change from the transient to the steady state operation condition, the impact of the instantaneous variation in the value of the reference current should be considered in the control loop of the DG unit so that:

$$\frac{dI_{refd}}{dt} = I_{avd}, \qquad \frac{dI_{refq}}{dt} = I_{avq} \tag{4.45}$$

By substituting (4.45) in (4.42) and (4.43), the switching state value of the interface system from the dynamic to the steady state condition can be expressed as:

$$d_{nd} = \frac{-v_m - R_c I_{refd} + \omega L_c I_{refq} - L_c I_{avd}}{v_r} \tag{4.46}$$

$$d_{nq} = \frac{-R_c I_{refq} - \omega L_c I_{refq} - L_c I_{avq}}{v_r} \tag{4.47}$$

By substituting the switching state function in (4.44), the following relationship is obtained:

$$\left(I_{refd} + \frac{L_c I_{avd} + v_m}{2R_c}\right)^2 + \left(I_{refq} + \frac{L_c I_{avq}}{2R_c}\right)^2 = \frac{(L_c I_{avd} + v_m)^2 + (L_c I_{avq})^2 + 4R_c v_r I_{dc}}{4R_c^2} \tag{4.48}$$

where (4.48), represents the mathematical relationship of the circle with a centre at $\left(-\left(\frac{L_c I_{avd}+v_m}{2R_c}\right), -\left(\frac{L_c I_{avq}}{2R_c}\right)\right)$ and a radius of $\sqrt{\frac{(L_c I_{avd}+v_m)^2+(L_c I_{avq})^2+4R_c v_r I_{dc}}{4R_c^2}}$ which represents the maximum capacity of the DG to compensate the active and reactive powers to the power grid in both a DC and AC conditions.

Figure 4.10 shows the comparison between the load and the DG current components, which clarifies the region that the DG can cover when the non-linear load is connected to the grid. Therefore, the interfaced DG system can cover the load current which lies inside the circuit, and it equals the maximum capacity of the interface system for the power injection.

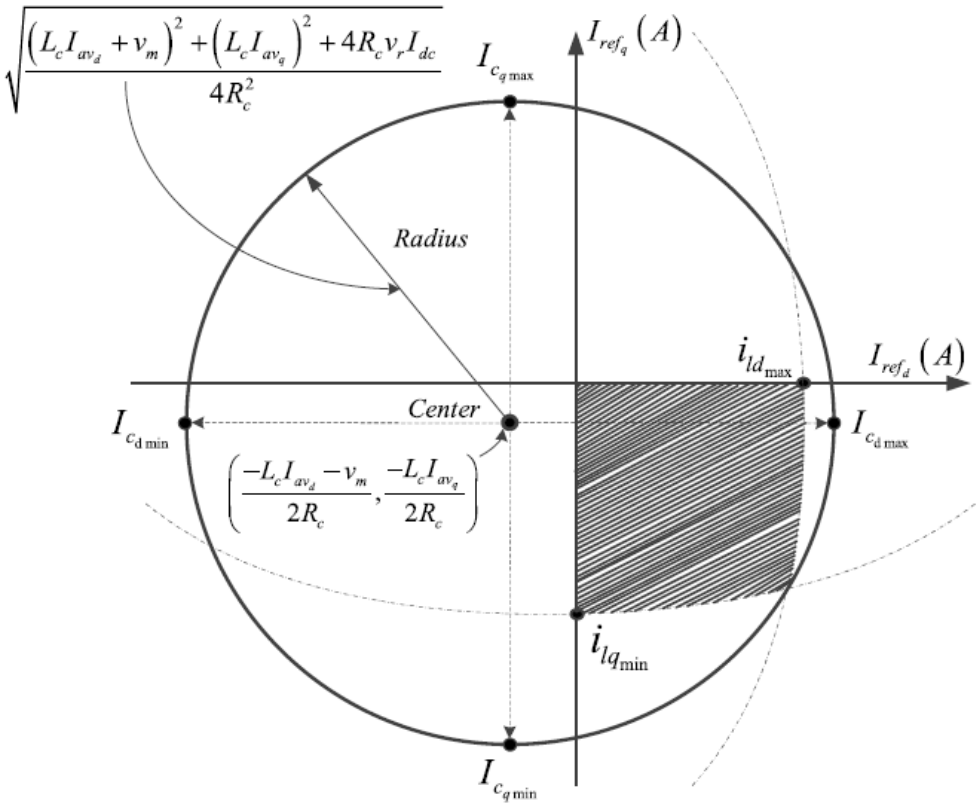

Fig. 4.10: The comparison between the load and DG current component

By assuming $i_{cd} = i_{ld}$, i_{cd} can be written as:

$$i_{cd} = \frac{-(L_c I_{avd} + v_m)}{2R_c} + \sqrt{\frac{(L_c I_{avd} + v_m)^2 + (L_c I_{avq})^2 + 4R_c v_r I_{cd}}{4R_c^2} - \left(i_{lq} + \frac{L_c I_{avq}}{2R_c}\right)^2}$$

Chapter 5

Simulation Results

In order to describe and test the performance of the proposed system, the overall control system is simulated using Matlab/Simulink environment; the schematic diagram of the proposed control system was shown in Fig. 4.9. The simulation parameters are given in the Table 5.1; the values are approximated to real system values obtained from industry.

The test model consists of the power converter with the maximum power rating 20kW connected to the grid that supplies a nonlinear load. A constant DC voltage source was considered as the source of the DG system. The capability of the control system in tracking the reference current with constant output active power are shown, and the ability of the system to provide the active and reactive powers. The harmonic current components of different loads are shown. The simulation result will be used to analyse the total harmonics distortion (THD) of the grid current before and after the DG is connected to the grid. In addition, the active power delivered from the DG to the power grid will be constant. By this assumption, it is possible to evaluate how the control system is able to track the fast change in the active and reactive power independently.

To simulate the real AC power grid, the nonlinear load is connected and disconnected randomly, and the grid current waveforms are measured under different situations.

Table 5.1*: Simulation Parameter.*

Parameter	**Value**
Grid voltage	400 V_{L-L}
dc-link voltage (v_{dc})	750 V
Fundamental frequency	50 Hz
Switching frequency	20 kHz

Coupling inductance (L_C)	0.5 mH
Coupling resistance (R_C)	0.1Ω
Line inductance (L_S)	0.1 mH
Line resistance (R_S)	0.1Ω
Nonlinear load resistance	20Ω
Nonlinear load inductance	1 mH
P_{ref}	20kW
Virtual inertia (J)	50kg*m^2
Damping coefficient (K_D)	7000

5.1 The Proposed VSG Test System

The system will be used to test the DG system consisting of the voltage source as the main source of the grid. At a frequency of 50 Hz, the transmission line is modelled as series inductance and resistance. The nonlinear load is represented by a full wave rectifier. The per phase load voltage is shown in Fig. 5.1, the small disturbance in the load voltage signal is caused by the nonlinear current drawn by the full wave rectifier. The phase current is shown in Fig. 5.2, the three phase voltages and currents are shown in the Fig. 5.3.

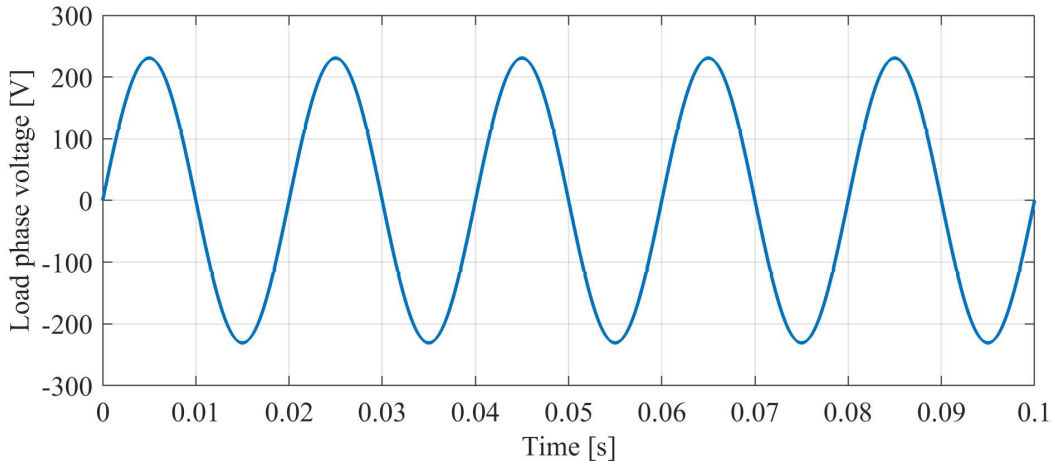

Fig. 5.1: The load voltage of the system

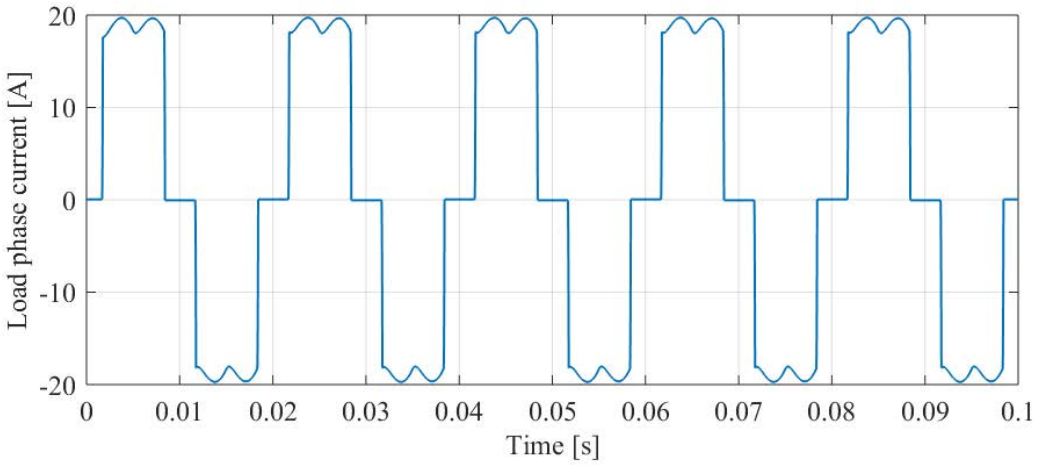

Fig. 5.2: The load current of the system

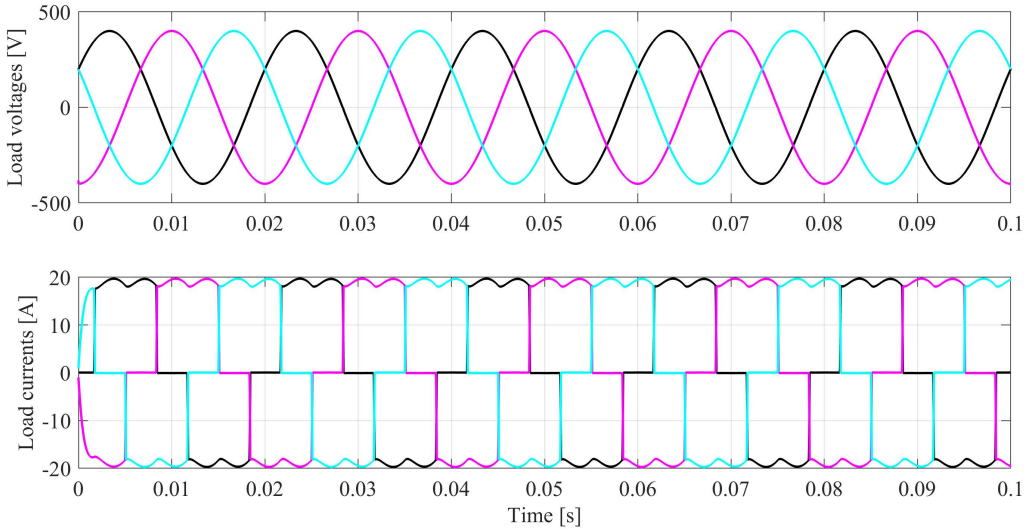

Fig. 5.3: The three phase currents and voltages of the load

5.2 VSG Operating as Active Power Filter

Figure 5.4 represents the load current, source current and VSG when it work as Active Power Filter (APF). The VSG is supply all the harmonic components of the load current, and the source current represent as pure sinewave signal. Fig. 5.5 represents the source voltage

and source current, the phase angle between the voltage and current show the power factor of the grid is not unite, this problem will be treate whent the VSG work as reactive power compensator(D-STATCOM).

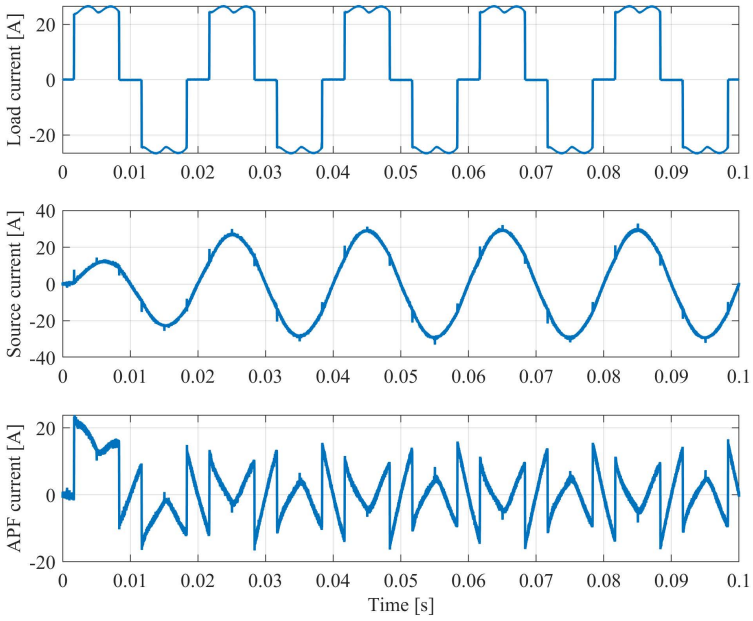

Fig. 5.4: The load current, source current and DG current after the DG work as Active Power Filter

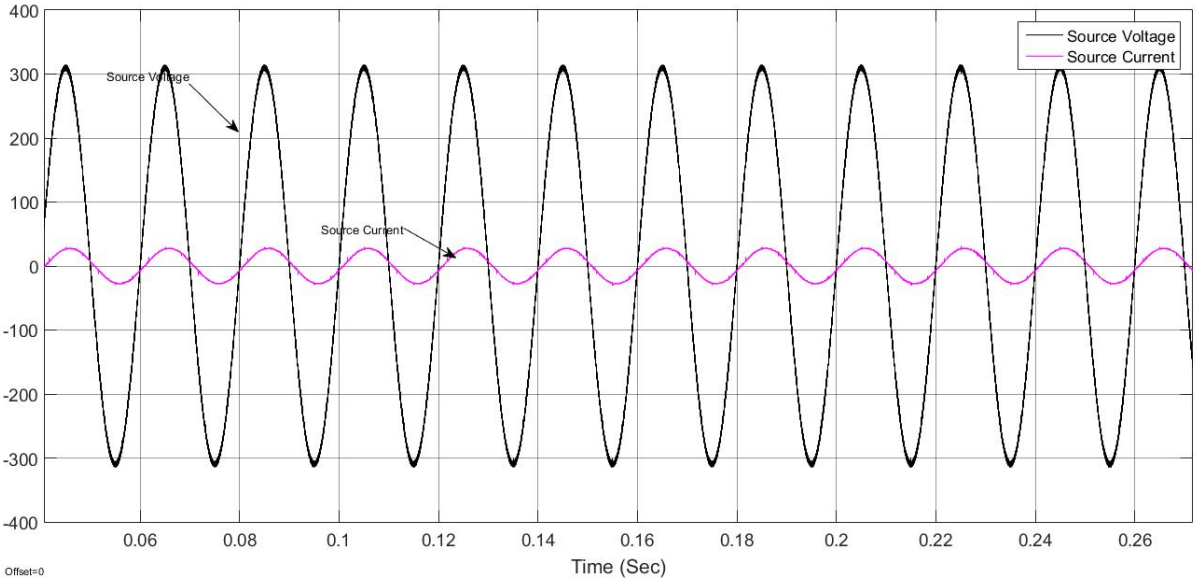

Fig. 5.5: *The grid voltage and current after the APF connect to the network*

5.3 VSG Operating as Active Filter and Reactive Power Compensator

The grid is connected to a load modelled by the full wave rectifier with per phase resistance 20Ω and inductance 10 mH. Fig. 5.6 shows the load voltage, load current, grid current and the DG current. At t=0.1s the DG link is connected to the network which supplies all the active and reactive power including the harmonic components to the load, at this situation the active power of the load is equal to the maximum active power of the DG, and the grid does not supply the current to the load ($i_{grid} = i_{load} - i_{DG}$). At t=0.2s, additional load is added to the network, at this situation the active power of the load is higher than the maximum active power rating of the DG. In this situation, the reactive power is injected by the DG and the grid injects the remaining active power. The grid supplies a current with high quality so the waveform is pure sinusoidal under the connection of the nonlinear load to the grid.

Fig. 5.7, shows the current and the voltage of the source after connecting the DG to the network. The voltage and current are in phase so the grid does not need to supply the reactive power to the load, and the reactive power is injected by the DG. The DG system makes the power factor of the grid unity (pf=1).

The ability of the DG control system to track the reference current in the d and q axis during the connection of the DG to the network and after adding the additional load to the grid is shown in Fig. 5.8 and Fig. 5.9. The harmonic and the dc components of the current in d-axis are shown in Fig. 5.10.

The ability of the DG control system to track the reference current in the d and q axis during the connection of the DG to the network and after adding the additional load to the grid is shown in Fig. 5.8 and Fig. 5.9. The harmonic and the dc components of the current in d-axis are shown in Fig. 5.10.

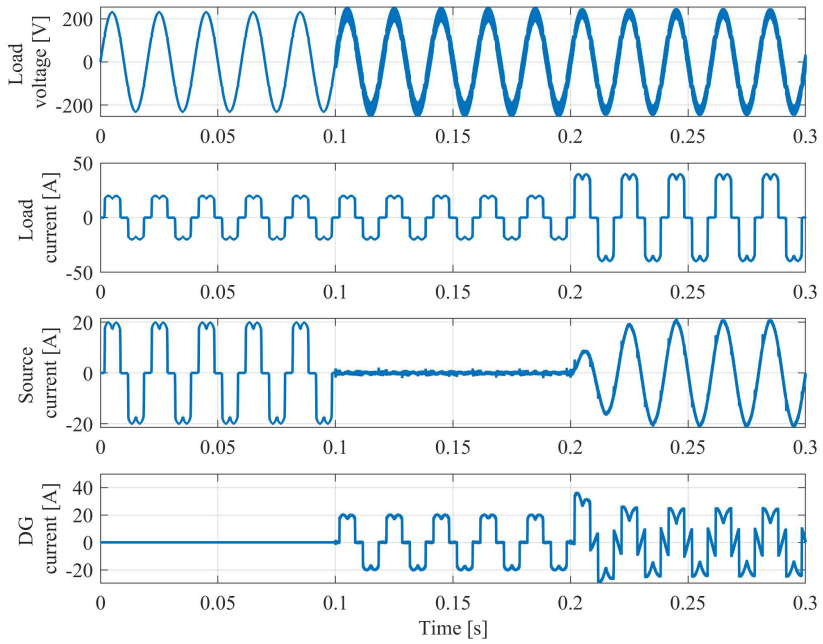

Fig. 5.6: The load voltage, load, grid, DG currents from top to bottom, respectively. The DG unit is connected at t=0.1s,at 0.2s additional load is connected to the grid

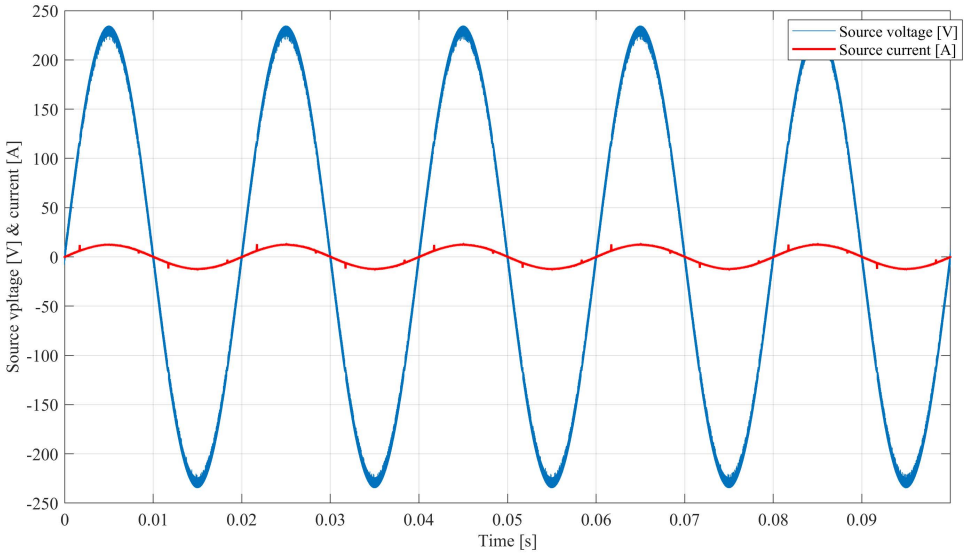

Fig. 5.7: The grid voltage and current before and after additional load connected to the grid

The ability of the DG control system to track the reference current in the d and q axis during the connection of the DG to the network and after adding the additional load to the grid is

shown in Fig. 5.8 and Fig. 5.9. The harmonic and the dc components of the current in d-axis are shown in Fig. 5.10.

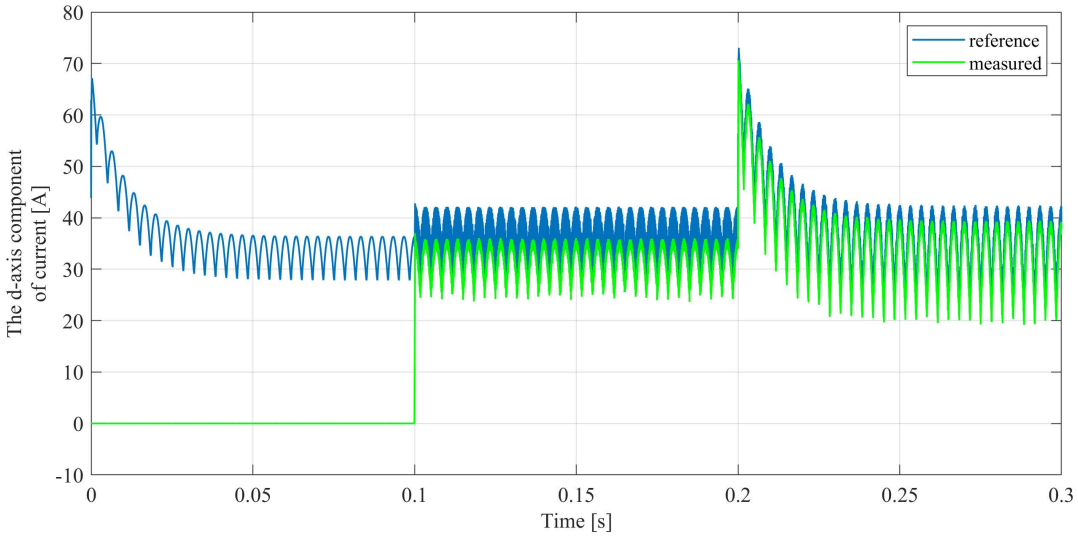

Fig. 5.8: The d axis reference current tracking the load current after connection the DG to the network and after additional load is connected to the grid

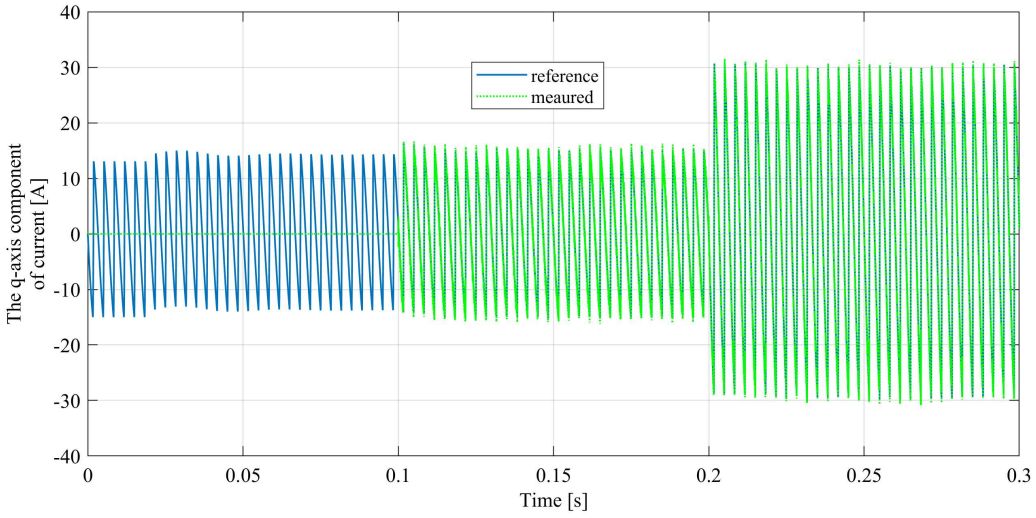

Fig. 5.9: The q-axis reference current tracking the load current after connecting the DG to the network and after additional load is connected to the grid

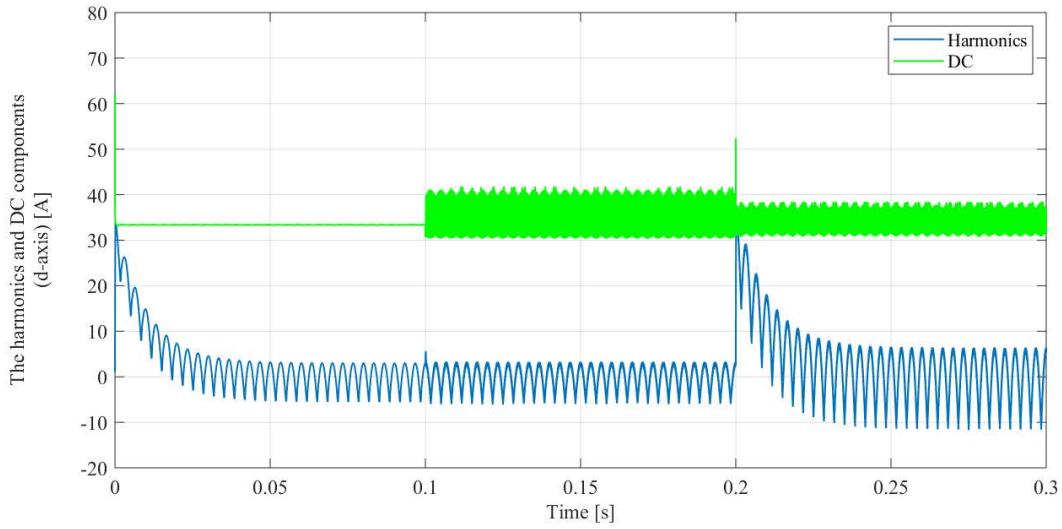

Fig. 5.10: The direct and harmonic components of the load in the d-axis

Figure 5.11, shows a comparison between the grid angles generated by the PLL and the angle generated from the virtual inertial implemented in the system. The result improve that the capability of the VSG to track the angle at the PCC.

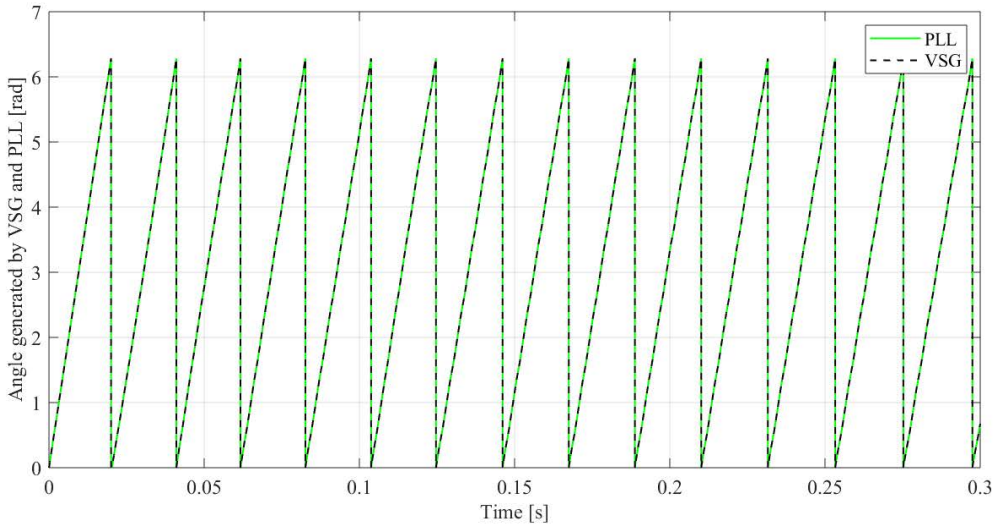

Fig. 5.11: The angle generated by the virtual inertia and by PLL

Figure 5.12, shows the active power of the load, source and DG link. Before the connection of the DG link, the active power is supplied by the grid. After the DG link connected to the network at t=0.1s, the active power generated by the grid is reduced to zero and it is injected by the DG. When the additional load is added to the network at t=0.2s, the DG is injecting the maximum active power and the remaining power is injected by the source.

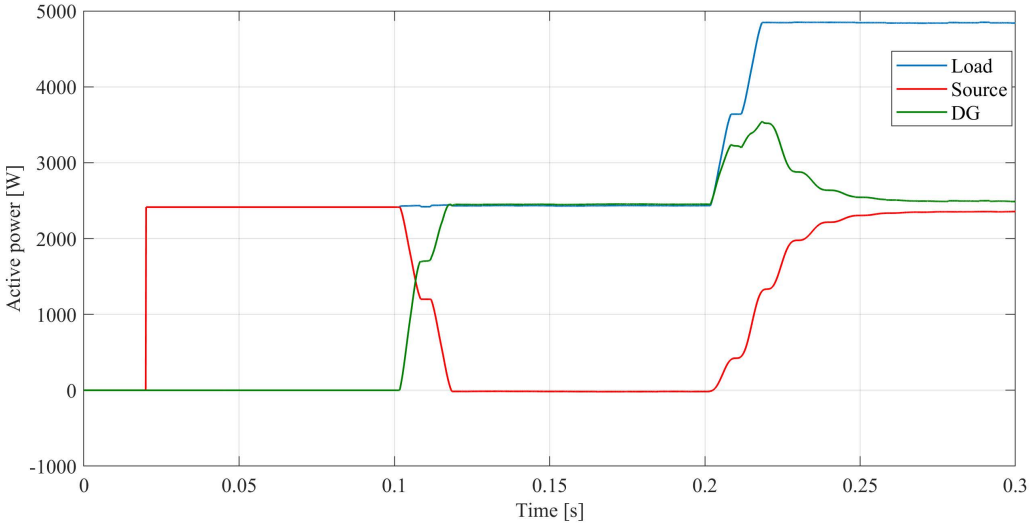

Fig. 5.12: The source, load and DG active power

Figure 5.13 shows the reactive power of the load, DG and grid. Before the connection of the DG to the network, the reactive power is supplied by the grid and after the DG is connected to the network, the reactive power of the grid is reduced to zero and it is supplied by the DG link.

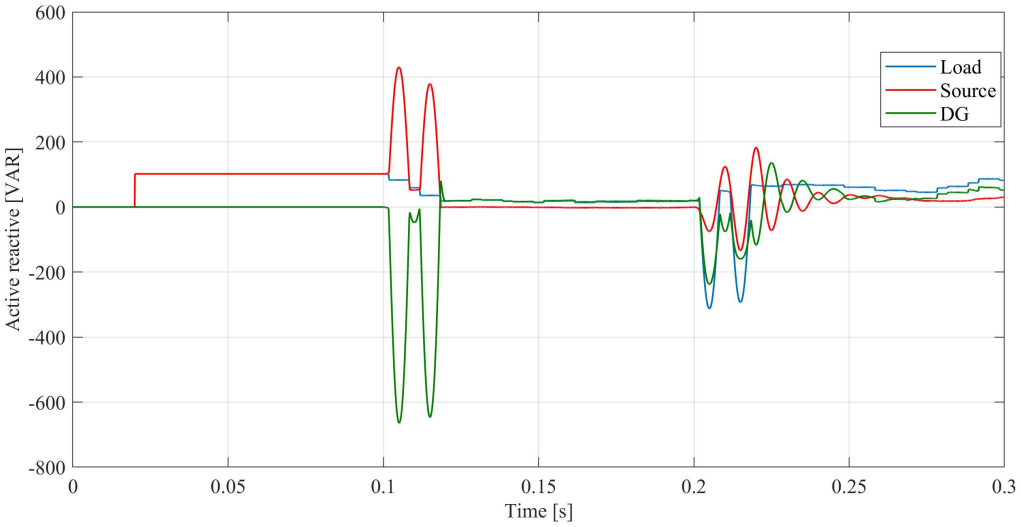

Fig. 5.13: The source, load and DG reactive power

5.4 VSG Operation When It is subjected to The Three Phase Fault Current

The load is subjected to the three phase fault currents within five cycles (0.1 sec) to test the capability of the VSG to maintain the frequency in the save range, and return back to the operation range after the faults is removed.

Fig. 5.14 represents the load current, source current and VSG current. At t=0.1s, the load is subjected to the three phase fault currents, and the fault is removed at t=0.2s. The capability of the VSG to return to the normal operation after the fault removed is shown.

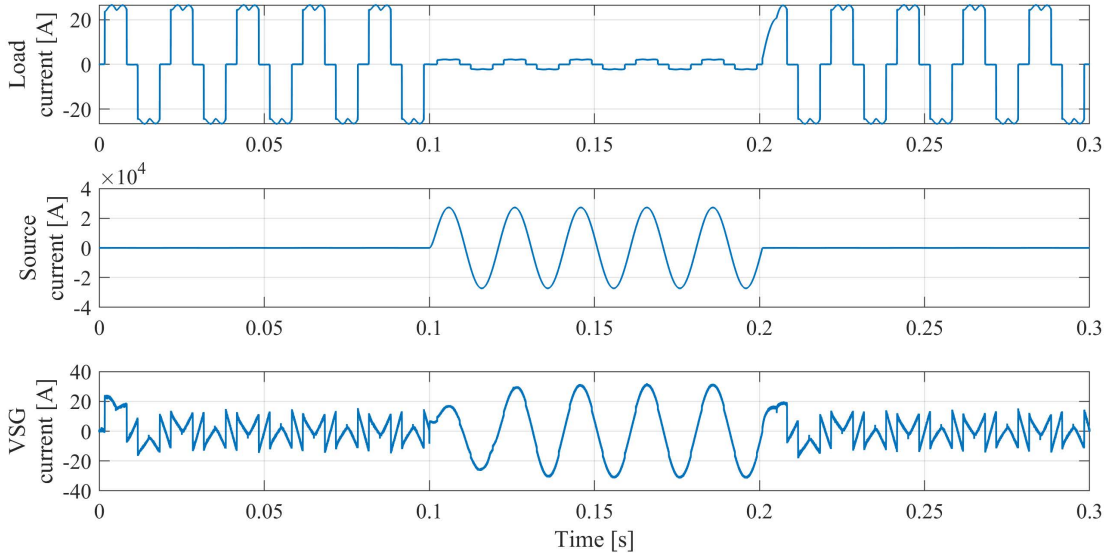

Fig. 5.14: The load, grid, VSG current when the load is subjected to the three phase fault currents

Fig. 5.15 represents the frequency of the current injected by the VSG before and after the system is subjected to the three-phase short circuit fault within five cycles. The frequency is slightly droped and returned to the steady state condition after the fault removed, the decrease of the frequency in the system depends on the amount of virtual inertia and the droop

coefficient of the swing equation. The response of the frequency does not change rapidly so that gives the system more stability under the challenge in the real network.

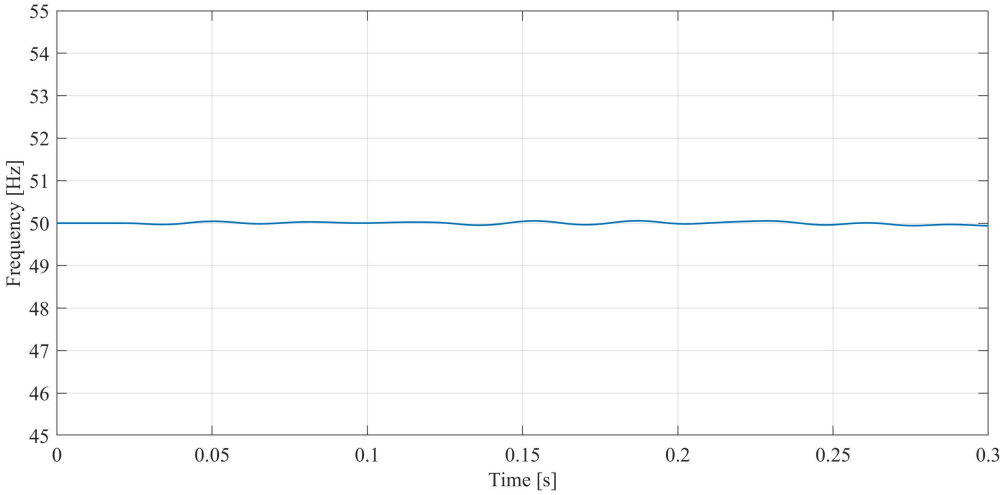

Fig. 5.15: The VSG current frequency when it subjected to the three phase short circuit fault

Chapter 6

Conclusion and Future Works

6.1 Conclusion

Multipurpose control algorithm for integration of the two level inverter based on the DG interface is presented. The proposed control algorithm makes the system more stable and produce high quality waveform supplied by the grid under the challenging of the real network. The control algorithm is designed based on analysing the load current into αβ and dq frame as mentioned before, the sinusoidal pulse width modulation (SPWM) was used to produce the gate signals of the semiconductor devices. The capability of the control system to produce the active and reactive power in the fundamental and harmonics is demonstrated. The capability curve of the interface signal to provide the active and reactive current in the d and q axis is presented, and the overall control diagram of the proposed control algorithm is presented.

The basic concepts of the synchronous generator are presented. The concept and control strategy of the VSG are introduced. Damping power and inertial emulation model are presented. The system is modelled using Matlab/Simulink environment to verify and improve the capability of the control system of the VSG.

6.2 Future works

The following guidelines are suggested to be done in the future:

- Coordination between VSGs and SGs, and revising the existing standard in the case of supporting frequency system needs further study.
- Implement all the components and features of the synchronous generator virtually in the control system of the VSG, included virtual impedance.
- Response of the frequency when the real power change and response of the voltage with respect to the reactive power change will be further study in this thesis.
- The effect of inertia on stability.
- The power sharing between two VSGs.

References

[1] I. Press, *Integration Of Distributed Generation In The Power Syatem*. IEEE Press, 2011.

[2] A. A. Abdelhafez, S. H. Alruways, Y. A. Alsaif, M. F. Althobaiti, A. B. Alotaibi, and N. A. Alotaibi, "Reactive Power Problem and Solutions : An Overview," pp. 40–54, 2017.

[3] Lakkireddy *et al.*, "State Voltage Stability Enhancement Using Shunt and Series FACTS Devices," in *Clemson University Power Systems Conference (PSC)*, pp. 1–5.

[4] Grady, W.M, Sanatoso, and S, "Understanding PowerSystem Harmonics," *IEEE Power ENG*, vol. 21, no. 11, pp. 8–11, 2004.

[5] T. Shintai, Y. Miura, and T. Ise, "Oscillation damping of a distributed generator using a virtual synchronous generator," *IEEE Trans. Power Deliv.*, vol. 29, no. 2, pp. 668–676, 2014.

[6] K. Visscher and S. W. H. De Haan, "Virtual Synchronous Machines (Vsg'S) for Frequency Stabilisation in Future Grids With a Significant Share of Decentralized Generation," in *Smart Grid for Distribution, 2008, IET-CIRED Seminar*, 2008, no. 0118, pp. 23–24.

[7] T. Vu Van *et al.*, "Virtual Synchronous Generator: An Element Of Future Grids," *IEEE PES Innov. Smart Grid Technol. Conf. Eur. ISGT Eur.*, pp. 1–7, 2010.

[8] M. Klein, G. J. Rogers, and P. Kundur, "A Fundamental Study of Inter-Area Oscillations in Power Systems," *IEEE Trans. Power Syst*, vol. 6, pp. 914–921, 1991.

[9] S. Eftekharnejad, V. Vittal, G. T. Heydt, B. Keel, and J. Loehr, "Small signal stability

assessment of power systems with increased penetration of photovoltaic generation: A case study," *IEEE Trans. Sustain. Energy*, vol. 4, pp. 960–967, 2014.

[10] B. Crowhurst, E. F. El-Saadany, L. El Chaar, and L. A. Lamont, "Single-phase grid-tie inverter control using DQ transform for active and reactive load power compensation," *PECon2010 - 2010 IEEE Int. Conf. Power Energy*, pp. 489–494, 2010.

[11] P. Bapaiah, "Power Quality Improvement by using DSTATCOM," *Int. J. Emerg. Trends Electr. Electron.*, vol. 2, no. 4, pp. 1–12, 2013.

[12] R. R. Wallace, "A Three-Phase Active Power Filter Operating with Fixed Switching Frequency for Reactive Power and Current Harmonic Compensation," *IEEE Trans. Ind. Electron.*, vol. 42, no. 4, pp. 402–408, 1995.

[13] E. Pouresmaeil, C. Miguel-Espinar, M. Massot-Campos, D. Montesinos-Miracle, and O. Gomis-Bellmunt, "A control technique for integration of DG units to the electrical networks," *IEEE Trans. Ind. Electron.*, vol. 60, no. 7, pp. 2881–2893, 2013.

[14] S. Naderi, E. Pouresmaeil, and W. D. Gao, "The frequency-independent control method for distributed generation systems," *Appl. Energy*, vol. 96, pp. 272–280, 2012.

[15] E. Rakhshani, D. Remon, A. M. Cantarellas, H. Mehrjerdi, and P. Rodriguez, "Derivative Based Inertia Emulation of Interconnected Systems Considering Phase-Locked Loop Dynamics," *IEEE Power Energy Soc. Gen. Meet.*, vol. 2016-Novem, no. 2, pp. 2–6, 2016.

[16] J. Liu, Y. Miura, and T. Ise, "Comparison of Dynamic Characteristics between Virtual Synchronous Generator and Droop Control in Inverter-Based Distributed Generators," *IEEE Trans. Power Electron.*, vol. 31, no. 5, pp. 3600–3611, 2016.

[17] H. Bevrani, T. Ise, and Y. Miura, "Virtual synchronous generators: A survey and new

perspectives," *Int. J. Electr. Power Energy Syst.*, vol. 54, pp. 244–254, 2014.

[18] J. Alipoor, Y. Miura, and T. Ise, "Power System Stabilization Using Virtual Synchronous Generator With Alternating Moment of Inertia," *IEEE J. Emerg. Sel. Top. POWER Electron.*, vol. 03, no. 2, pp. 451–458, 2015.

[19] M. Guan, W. Pan, J. Zhang, Q. Hao, J. Cheng, and X. Zheng, "Synchronous Generator Emulation Control Strategy for Voltage Source Converter (VSC) Stations," *IEEE Trans. Power Syst.*, vol. 30, no. 6, pp. 3093–3101, 2015.

[20] S. D'Arco, J. A. Suul, and O. B. Fosso, "Small-signal modelling and parametric sensitivity of a Virtual Synchronous Machine," in *Power Systems Computation Conference, PSCC 2014*, 2014, pp. 18–22.

[21] D. Remon, A. M. Cantarellas, E. Rakhshani, I. Candela, and P. Rodriguez, "An active power self-synchronizing controller for grid-connected converters emulating inertia," in *3rd International Conference on Renewable Energy Research and Applications, ICRERA 2014*, 2014, pp. 424–429.

[22] J. Alipoor, Y. Miura, and T. Ise, "Distributed generation grid integration using virtual synchronous generator with adoptive virtual inertia," *Energy Convers. Congr. Expo.*, pp. 4546–4552, 2013.

[23] Y. Chen, R. Hesse, D. Turschner, and H. P. Beck, "Investigation of the virtual synchronous machine in the island mode," *IEEE PES Innov. Smart Grid Technol. Conf. Eur.*, pp. 1–6, 2012.

[24] Y. Hirase, K. Abe, O. Noro, K. Sugimoto, and K. Sakimoto, "Stabilization effect of virtual synchronous generators in microgrids with highly penetrated renewable energies," *2016 IEEE 17th Work. Control Model. Power Electron. COMPEL 2016*,

2016.

[25] Y. Chen, R. Hesse, D. Turschner, and H. Beck, “Dynamic Properties of the Virtual Synchronous Machine (VISMA),” *Proc. ICREPQ*, vol. 1, no. 9, pp. 1–5, 2011.

[26] Y. Chen, R. Hesse, D. Turschner, and H. P. Beck, “Improving the grid power quality using virtual synchronous machines,” in *2011 International Conference on Power Engineering, Energy and Electrical Drives*, 2011, pp. 1–6.

[27] M. P. N. Van Wesenbeeck, S. W. H. De Haan, P. Varela, and K. Visscher, “Grid tied converter with virtual kinetic storage,” in *2009 IEEE Bucharest PowerTech: Innovative Ideas Toward the Electrical Grid of the Future*, 2009, no. 1, pp. 1–7.

[28] R. Hesse, D. Turschner, and H. Beck, “Micro Grid Stabilization Using the Virtual Synchronous Machine (VISMA),” in *International Conferance Renewable Energy and Power Qulity (ICREPQ09)*, 2009.

[29] N. Mohan, T. M. M. Undeland, and W. P. Robbins, *Power Electronics: Converter, Application, and Design*, 3rd ed. WILLEY, 2002.

[30] I. BATARSEH, *POWER ELECTRONIC CIRCUITS*. United States of America: John Wiley & Sons Ltd, 2014.

[31] N. I. Raju, S. Islam, and A. A. Uddin, “Sinusoidal PWM Signal Generation Technique for Three Phase Voltage Source Inverter with Analog Circuit & Simulation of PWM Inverter for Standalone Load & Micro-grid System,” *Int. J. Renew. ENERGY Res.*, vol. 3, no. 3, pp. 647–658.

[32] K. Kim, “Filter design for grid connected PV inverters,” 2008, no. December, pp. 1201–1206.

[33] T. C. Wang, Z. Ye, G. Sinha, and X. Yuan, “Output Filter Design for a Grid-

interconnected Three-Phase Inverter," in *vol.2*, pp. 779–784.

[34] S. T. G. Power *et al.*, "Analysis of Phase-Locked Loop Low-Frequency Converters Considering Impedance Interactions," *IEEE Trans. Ind. Electron.*, vol. 62, no. 1, pp. 310–321, 2015.

[35] F. Blaabjerg, R. Teodorescu, S. Member, M. Liserre, A. V Timbus, and S. Member, "Overview of Control and Grid Synchronization for Distributed Power Generation Systems," vol. 53, no. 5, pp. 1398–1409, 2006.

[36] C. Venkatesh, D. S. Kumar, S. Members, D. V. S. S. S. Sarma, S. Member, and M. Sydulu, "Modelling of Nonlinear Loads and Estimation of Harmonics in Industrial Distribution System," vol. 2, no. December, pp. 592–597, 2008.

[37] Z. Kai and C. Liuchen, "Harmonic current reduction for a PWM rectifier with very low carrier ratio in a microturbine system," *Can. Conf. Electr. Comput. Eng.*, vol. 2005, no. May, pp. 587–590, 2005.

[38] B. Y. R. H. Park, "Two Reaction Theory of Synchronous Machines Generalized Method of Analysis-Part I," pp. 716–727, 1929.

[39] M. A. X. W. Schulz and E. Clarke, "Determination of Instantaneous Currents and Voltages by Means of Alpha , Beta ," *AJEE Trans.*, pp. 1248–1255, 1951.

[40] J. F. Silva, "Space Vector Alfa Beta Current Regulator for Sliding Mode Controlled Unity Power Factor PWM Rectifiers," *IEEE*, no. 24, pp. 1877–1882, 1998.

[41] N. Pogaku, M. Prodanović, and T. C. Green, "Modeling, analysis and testing of autonomous operation of an inverter-based microgrid," *IEEE Trans. Power Electron.*, vol. 22, no. 2, pp. 613–625, 2007.

[42] M. P. Kazmierkowski and L. Malesani, "Current control techniques for three-phase

voltage-source PWM\nconverters: a survey," *IEEE Trans. Ind. Electron.*, vol. 45, no. 5, pp. 691–703, 1998.

[43] M. P. Kaimierkowski and W. Sulkowski, "Novel space vector based current controllers for PWM-inverters - Power Electronics, IEEE Transactions on," *IEEE Trans. POWER Electron.*, vol. 6, no. I, pp. 158–166, 1991.

[44] E. Pouresmaeil, M. Mehrasa, and J. P. S. Catalão, "A multifunction control strategy for the stable operation of DG units in smart grids," *IEEE Trans. Smart Grid*, vol. 6, no. 2, pp. 598–607, 2015.

[45] Y. Dai, H. Wang, and G. Zeng, "Double Closed-Loop PI Control of Three-Phase Inverters by Binary-Coded Extremal Optimization," *IEEE Access*, vol. 4, pp. 7621–7632, 2016.

[46] D. Stojic, T. Tarczewski, and I. Klasnic, "Proportional-Integral-Resonant AC Current Controller," *Adv. Electr. Comput. Eng.*, vol. 17, no. 1, pp. 8–9, 2017.

[47] N. Zhang, H. Tang, and C. Yao, "A Systematic Method for Designing a PR Controller and Active Damping of the LCL Filter for Single-Phase Grid-Connected PV Inverters," *energies*, vol. 7, pp. 3934–3954, 2014.

[48] D. Zammit, C. S. Staines, M. Apap, and J. Licari, "Design of PR current control with selective harmonic compensators using Matlab," *J. Electr. Syst. Inf. Technol.*, vol. 4, no. 3, pp. 347–358, 2017.

[49] R. Zhang, M. Cardinal, P. Szczesny, and M. Dame, "A Grid Simulator with control of single-phase power converters in D-Q rotating frame," *PESC Rec. Annu. Power Electron. Spec. Conf.*, vol. 3, pp. 1431–1437, 2002.

[50] P. Santiprapan, K. Areerak, and K. Areerak, "Mathematical Model and Control

Strategy on DQ Frame for Shunt Active Power Filters," vol. 5, no. 12, pp. 1664–1672, 2011.

[51] T. Sutikno and M. Facta, "An Efficient Strategy to Generate High Resolution Three-Phase Pulse Width Modulation Signal Based on Field Programmable Gate Array," *Int. J. Comput. Electr. Eng.*, vol. 2, no. 3, pp. 3–6, 2010.

[52] S. J Chapman, *Electrical Machinery Fundamentals*, 5th ed. McGraw, 2005.

[53] M. Jan, B. J. W, and B. J. R, *Power System Dynamics Stability and Control*. John Wiley & Sons Ltd, 2009.

[54] P. Basu and A. Harichandan, "Power System Stability Studies Using Matlab," pp. 1–110, 2009.

[55] M. S. S. Seshu Babu and M. S. S. Sriram, "Current Control Technique For Grid Connected Distributed Generation (DG) Resources Using ANN controller," *Int. J. Sci. Eng. Adv. Technol.*, vol. 3, no. 12, pp. 1261–1269, 2015.

[56] "Advance Control of Multilevel Converters for Integration of Distributed Generation Resources into AC Grid," 1996.

Appendix A Matlab/ Simulink Models

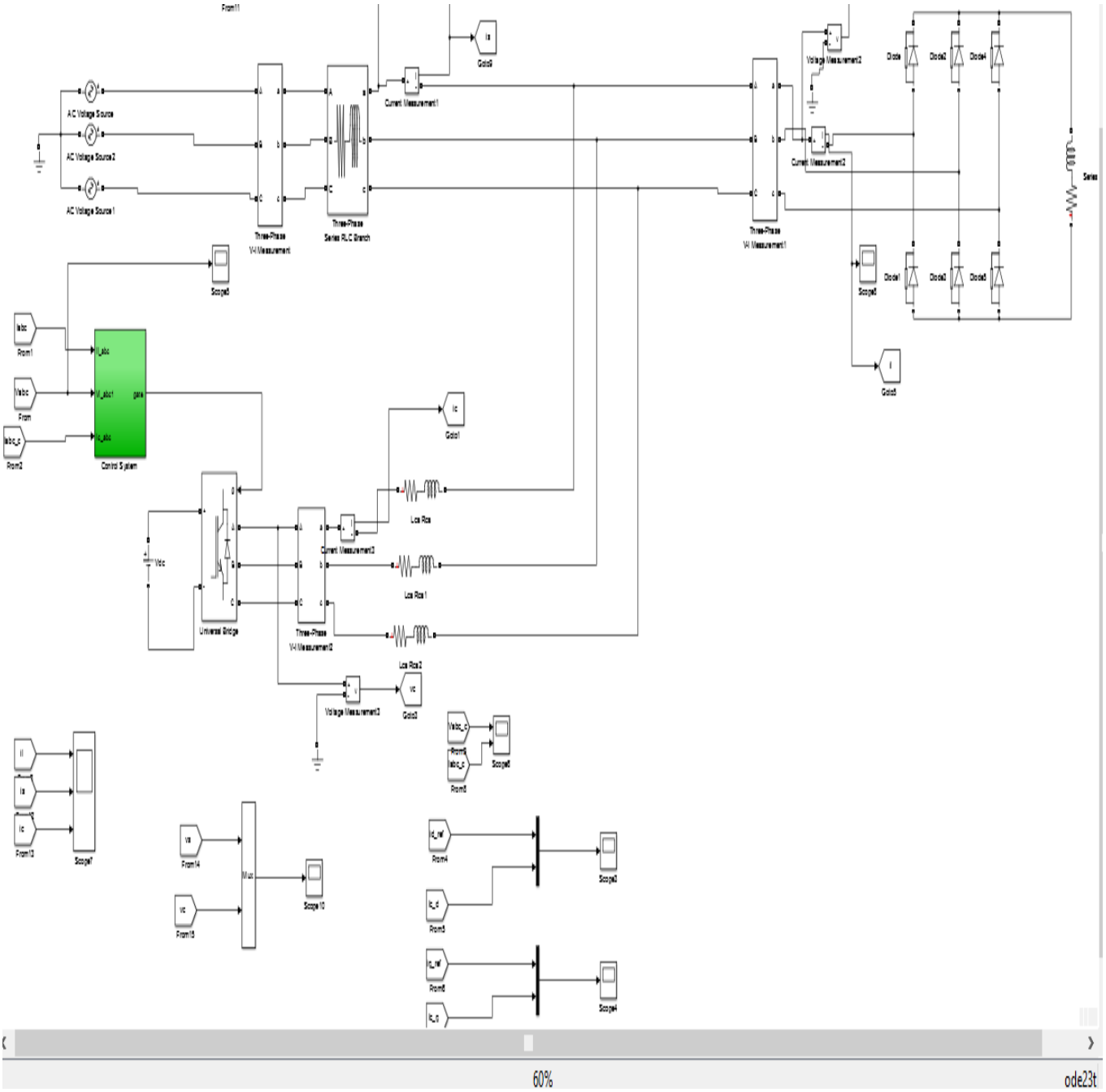

Overall Control System

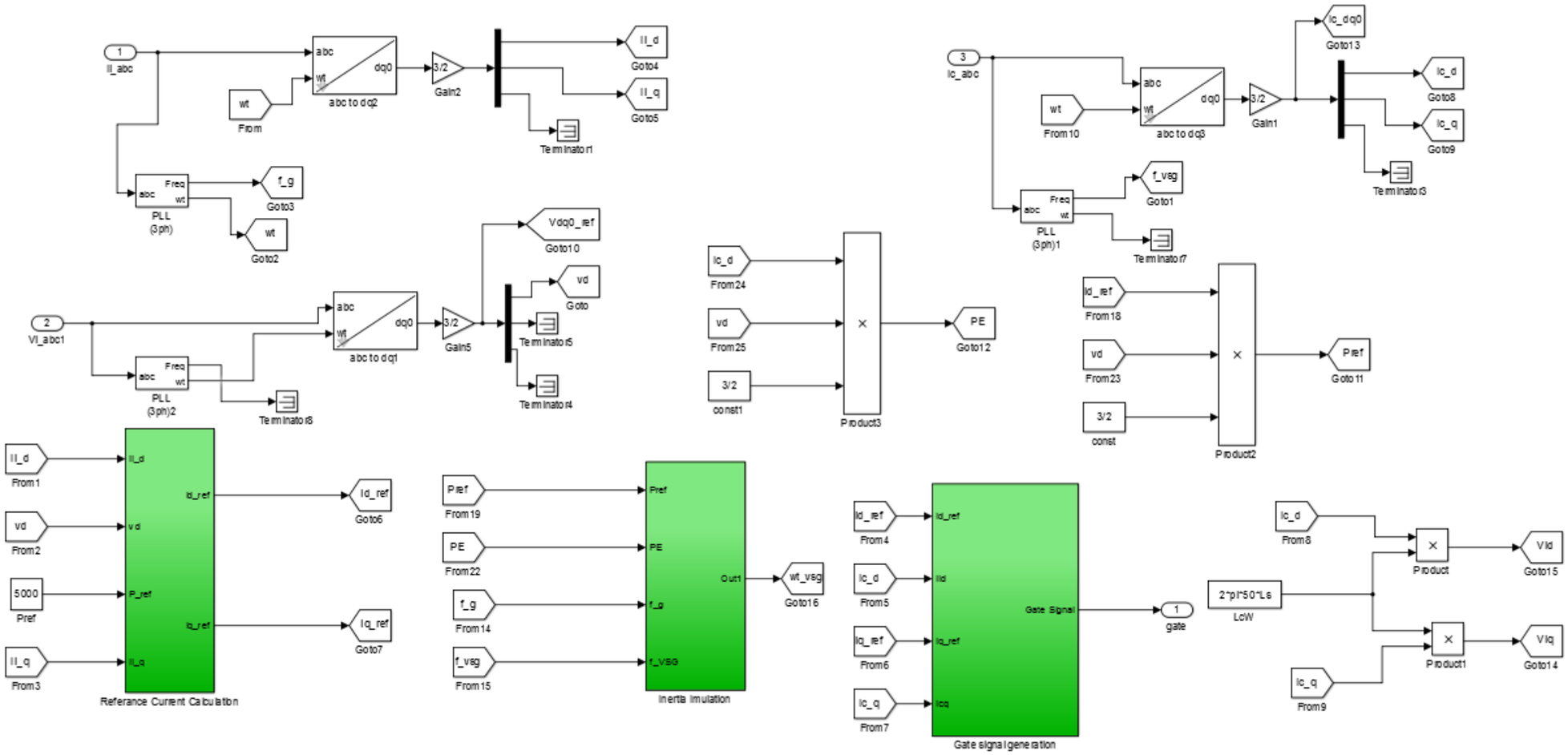

Reference Current Calculation

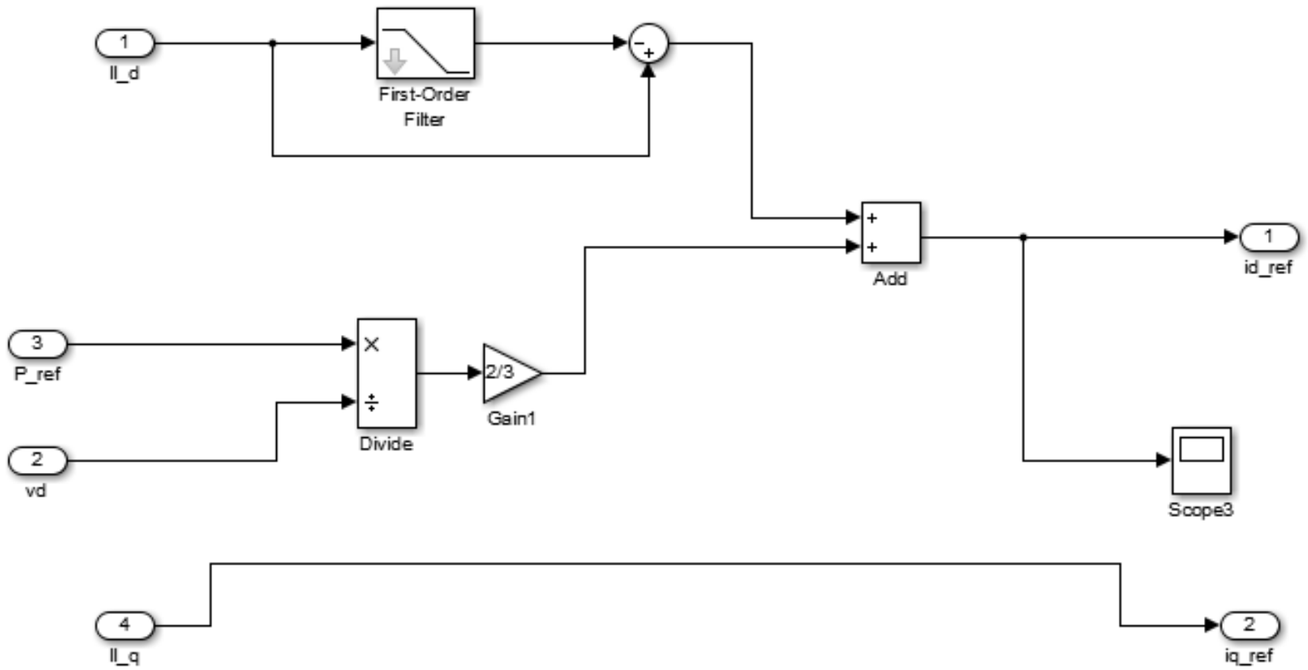

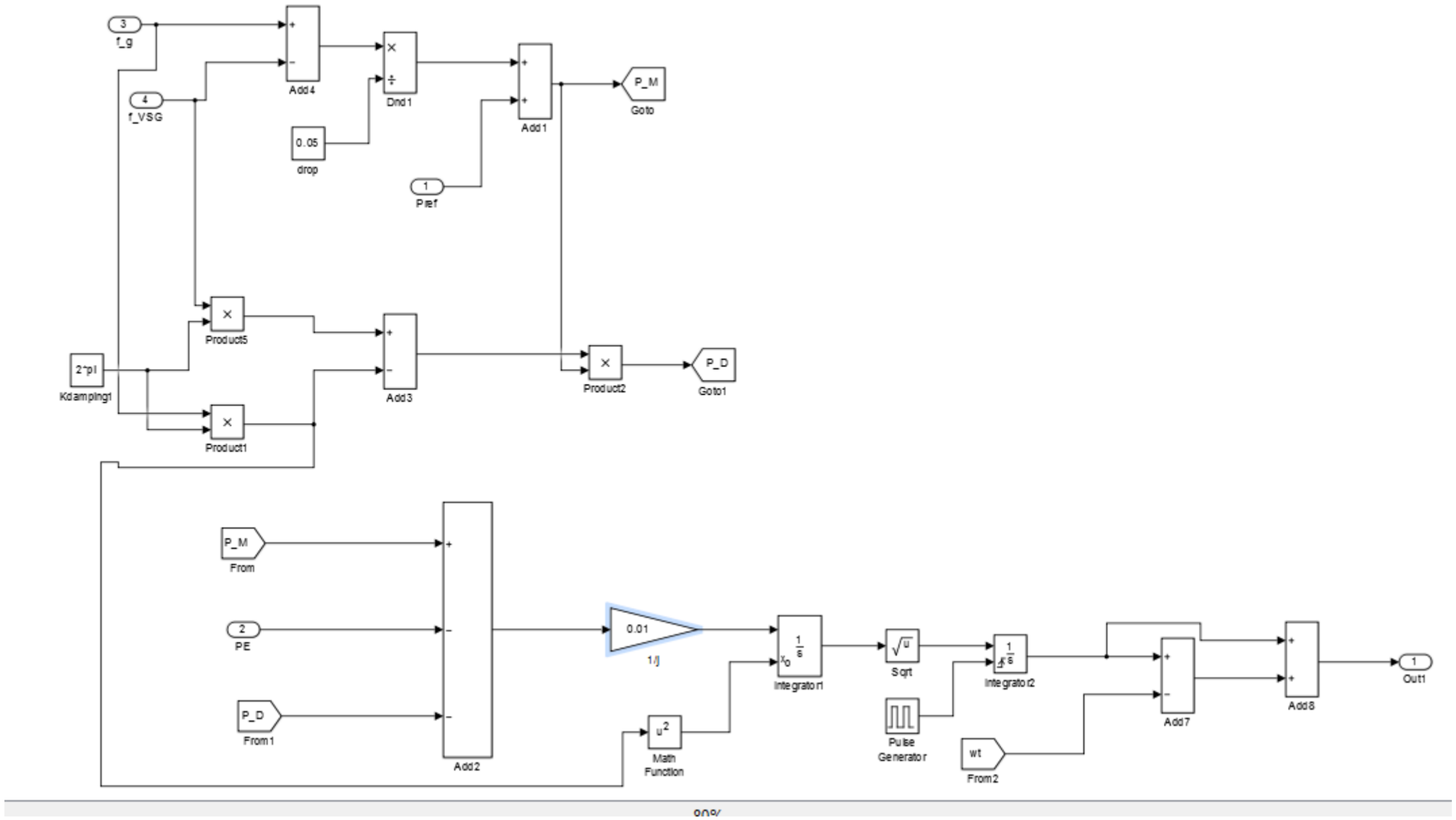
3
f_g
4
f_VSG
Add4
Dnd1
0.05
drop
Add1
P_M
Goto
1
Pref
Product5
2*pi
Kdamping1
Add3
Product2
P_D
Goto1
Product1
P_M
From
2
PE
P_D
From1
Add2
0.01
1/j
Integrator1
Sqrt
Integrator2
Add7
Add8
1
Out1
Pulse
Generator
wt
From2
Math
Function

Gate signal generation